Earth and Planetary Science Letters 481 (2018) 48–60

Contents lists available at ScienceDirect

Earth and Planetary Science Letters

www.elsevier.com/locate/epsl

Controls over $\delta^{44/40}$Ca and Sr/Ca variations in coccoliths: New perspectives from laboratory cultures and cellular models

Luz María Mejía [a,b,*], Adina Paytan [c], Anton Eisenhauer [d], Florian Böhm [d], Ana Kolevica [d], Clara Bolton [a,1], Ana Méndez-Vicente [a], Lorena Abrevaya [a], Kirsten Isensee [a,2], Heather Stoll [a,b,*]

[a] Dept. Geología, Universidad de Oviedo, Arias de Velasco s/n, 33005 Oviedo, Asturias, Spain
[b] Geological Institute, Department of Earth Science, Sonneggstrasse 5, ETH, 8092, Zürich, Switzerland
[c] Institute of Marine Sciences, University of California, Santa Cruz, 1156 High St., Santa Cruz, CA, USA
[d] GEOMAR Helmholtz Zentrum für Ozeanforschung Kiel, Wischhofstrasse 1-3, 24148 Kiel, Germany

ARTICLE INFO

Article history:
Received 14 October 2016
Received in revised form 5 October 2017
Accepted 6 October 2017
Available online xxxx
Editor: M. Bickle

Keywords:
coccolithophores
calcium isotopes
coccolith calcification
Ca isotopic fractionation
desolvation
CaSri–Co model

ABSTRACT

Coccoliths comprise a major fraction of the global carbonate sink. Therefore, changes in coccolithophores' Ca isotopic fractionation could affect seawater Ca isotopic composition, affecting interpretations of the global Ca cycle and related changes in seawater chemistry and climate. Despite this, a quantitative interpretation of coccolith Ca isotopic fractionation and a clear understanding of the mechanisms driving it are not yet available. Here, we address this gap in knowledge by developing a simple model (CaSri–Co) to track coccolith Ca isotopic fractionation during cellular Ca uptake and allocation to calcification. We then apply it to published and new $\delta^{44/40}$Ca and Sr/Ca data of cultured coccolithophores of the species *Emiliania huxleyi* and *Gephyrocapsa oceanica*. We identify changes in calcification rates, Ca retention efficiency and solvation–desolvation rates as major drivers of the Ca isotopic fractionation and Sr/Ca variations observed in cultures. Higher calcification rates, higher Ca retention efficiencies and lower solvation–desolvation rates increase both coccolith Ca isotopic fractionation and Sr/Ca. Coccolith Ca isotopic fractionation is most sensitive to changes in solvation–desolvation rates. Changes in Ca retention efficiency may be a major driver of coccolith Sr/Ca variations in cultures. We suggest that substantial changes in the water structure strength caused by past changes in temperature could have induced significant changes in coccolithophores' Ca isotopic fractionation, potentially having some influence on seawater Ca isotopic composition. We also suggest a potential effect on Ca isotopic fractionation via modification of the solvation environment through cellular exudates, a hypothesis that remains to be tested.

1. Introduction

Coccolithophores are marine unicellular calcifying phytoplankton, responsible for a large fraction of the $CaCO_3$ export to the deep ocean. Although their contribution to global primary productivity is small compared to other phytoplankton, coccolithophores are key modulators of the carbon cycle, accounting for ~50% of the $CaCO_3$ sediment production in the modern ocean (Milliman, 1993) and as much as ~95% of the pelagic $CaCO_3$ in the earliest Cenozoic. Variability in coccolithophores' contribution to $CaCO_3$ burial or their Ca isotopic fractionation could have the potential to impact seawater Ca isotopic composition ($\delta^{44/40}$Ca) over time, affecting the interpretation of the $\delta^{44/40}$Ca record in terms of the global Ca cycle (Fantle, 2010). The study of coccolith $\delta^{44/40}$Ca may provide important information not only about the past Ca cycle, but also about the physiological response of coccolithophores regarding Ca uptake and allocation to the calcification process under changing ocean chemistry and environmental conditions.

Culture experiments under variable temperature, carbonate chemistry, light, salinity and Ca and Mg concentrations have documented variation in Ca isotopic fractionation in coccolithophores (Gussone et al., 2007, 2006; Langer et al., 2007; Müller et al., 2011), which could translate into variations in Ca isotopic fractionation of this part of the carbonate sink. Gussone et al. (2006)

* Corresponding authors at: Geological Institute, Department of Earth Science, Sonneggstrasse 5, ETH, 8092, Zürich, Switzerland.
E-mail address: luz.mejia@erdw.ethz.ch (L.M. Mejía).
[1] Present address: Aix-Marseille Université, CNRS, IRD, CEREGE UM34, 13545 Aix en Provence, France.
[2] Present address: UNESCO Intergovernmental Ocean Commission, 1 rue Miollis, 75732 Paris cedex 15, France.

https://doi.org/10.1016/j.epsl.2017.10.013
0012-821X/

proposed the first conceptual model of Ca isotopic fractionation in coccolithophores and suggested Ca dehydration during uptake across the plasma membrane to be responsible for the observed Ca isotopic fractionation. This Ca dehydration concept is equivalent to the more widely-used concept of desolvation, i.e. the removal of the solvent (in this case water) from the solute (in this case Ca) (Camacho et al., 2000). Desolvation is a key process controlling solute (e.g. proteins) transmembrane transport (e.g. Burton et al., 1992; Conradi et al., 1991). Although fractionation during desolvation has not yet been evaluated experimentally, molecular dynamic calculations have simulated a maximum fractionation of Ca isotopes during desolvation of −4.7‰ in solutions at infinite dilution, given the higher reactivity of the light calcium isotope (^{40}Ca) (Hofmann et al., 2012).

To identify the processes responsible for Ca isotopic fractionation in coccolithophores, here we implement the modeled potential for Ca isotopic fractionation during desolvation, in a new steady-state mass balance geochemical model of cellular Ca uptake and allocation to calcification in coccolithophores (CaSri–Co). We apply the model to interpret new coccolith $\delta^{44/40}$Ca and Sr/Ca results from *Emiliania huxleyi* and *Gephyrocapsa oceanica* cultured at varying CO_2 concentrations, as well as cultured *E. huxleyi* from previous studies (Gussone et al., 2006; Langer et al., 2007; Müller et al., 2011). The model elucidates how calcification rates, Ca retention efficiency, and the solvation environment properties control Ca isotopic fractionation and Sr/Ca in coccolithophores.

2. Materials and methods

2.1. Culture of coccolithophores

Coccolithophores of the species *E. huxleyi* (strain RCC 1216), *C. leptoporus* (strain RCC 1169) and *G. oceanica* (strain RCC 1292) were grown at Universidad de Oviedo at 18 °C on a 16/8 h light/dark cycle. Natural seawater for culturing was retrieved in the Cantabrian Sea during sampling campaigns in open waters 20 km from the coast. Seawater was enriched in nutrients according to the K/5 recipe (Keller et al., 1987), which contains no additional Ca or Sr. Cultures were acclimated to the experimental conditions for at least 6 generations, maintained in suspension by a continuous rolling system, and harvested at low cell density (<1.6 µg POC/mL) (Table 1). In pH manipulations, seawater carbonate chemistry was modified with the addition of 0.5 mol/L NaOH/HCl. In an additional experiment for *E. huxleyi*, seawater was acidified to remove dissolved inorganic carbon (DIC), and subsequently $NaHCO_3$ was added to adjust DIC to three different concentrations. None of the described methods for culture manipulation are expected to have affected the Ca concentration nor the Ca isotopic composition of the seawater used for culturing.

Total alkalinity (TA), pH, cell counts and growth rates were measured following standard procedures (Trimborn et al., 2009). The carbonate system was determined using CO_2 sys (Lewis and Wallace, 1998), applying equilibrium constants from Mehrbach et al. (1973) refitted by Dickson and Millero (1987). Carbon isotopic composition (δ^{13}C) of the media was analyzed at the time of cell harvest based on a continuous flow method similar to that described by Spötl (2005) using a gas preparation system GasPrep coupled to a Nu Instruments Horizon IRMS.

Cells were harvested for particulate organic carbon (POC) analysis on pre-combusted GF/F or QF/F filters and for particulate inorganic carbon (PIC) analysis on polycarbonate filters. PIC was determined by Ca yield using simultaneous dual inductively coupled plasma-atomic emission spectroscopy (ICP-AES, Thermo ICAP DUO 6300), following acidification with 2% HNO_3, except for *C. leptoporus*, where high Ca levels in blank filters precluded reliable determination of PIC. Ca depletion in the media remained <0.2% (Table 1), suggesting no significant changes of solution $\delta^{44/40}$Ca. Applying Rayleigh fractionation (Zeebe and Wolf-Gladrow, 2001), this maximum 0.2% in Ca depletion implies a maximum bias of 0.003‰ in our Ca isotopic fractionations, a value that is well below the error of measurements.

Cellular carbon quotas (organic carbon/cell, POC) were measured by flash combustion Elemental Analyzer (Euro Vector EA-1108) at 1020 °C coupled with a gas source isotope ratio mass spectrometer (Nu Instruments). Cell diameter and surface area are derived from cellular POC quotas using the regressions of Popp et al. (1998) since cellular carbon quotas scale predictably with biovolume. To compare calcification and Ca uptake among cells of different sizes, calcification rates were normalized to cell surface area.

δ^{13}C analyses were conducted to determine if there was any correlation between carbon and calcium isotopic fractionation. For $\delta^{44/40}$Ca and δ^{13}C analyses, harvesting was conducted on polycarbonate filters and cells were rinsed with high purity (Milli-Q) deionized distilled water and centrifuged to eliminate salt residues. For $\delta^{44/40}$Ca analysis, organic matter was oxidized following the method used in Stoll et al. (2012), with multiple steps of hot alkaline H_2O_2 solution. For δ^{13}C analysis, oxidation of organic matter was conducted following the method of Bairbakhish et al. (1999). Coccolith δ^{13}C was measured on a Nu Instruments Perspective dual-inlet isotope ratio mass spectrometer (DI-IRMS) connected to an automated carbonate preparation system (NuCarb) at the Universidad de Oviedo. Mean reproducibility of δ^{13}C was 0.05‰ (1σ). Carbon isotopic fractionation between the media DIC and the coccolith calcite ($\varepsilon_{coccolith}$) was calculated using the measured seawater media δ^{13}C of DIC at the end of the experiments. We use the term ε to refer to isotopic fractionation of *carbon*, while the term Δ is used to refer to isotopic fractionation of *calcium*.

2.2. Sample preparation for coccolith $\delta^{44/40}$Ca and Sr/Ca analysis

Coccolith calcite (~3–5 mg) was gently dissolved in weak 0.4 M acetic acid (~15–20 min). Splits of the $CaCO_3$ solution were used to determine Ca concentration and Sr/Ca ratios via dual inductively coupled plasma-atomic emission spectroscopy (ICP-AES) (Thermo ICAP DUO 6300) calibrated using the intensity ratio method, as described in Mejía et al. (2014).

For coccolith $\delta^{44/40}$Ca analysis, 120 µL of ^{43}Ca–^{48}Ca double spike was mixed with an aliquot of sample containing 3000 ng of Ca in pre-cleaned teflon beakers. After evaporation of the solution at ~100 °C, samples were reconstituted in 2.2 N HCl prior to analysis. For samples in which interfering compounds were affecting the isotope analysis due to isobaric interferences (e.g. $^{40}K^{+}$, $^{24}Mg^{19}F^{+}$, $^{25}Mg^{19}F^{+}$, $^{48}Ti^{+}$), Ca was purified and separated from other elements using column chemistry as previously described in Griffith et al. (2008).

2.3. Coccolith $\delta^{44/40}$Ca analysis

An aliquot of ~300 ng Ca loaded on an outgassed zone-refined Re filament was used for coccolith $\delta^{44/40}$Ca determination on a Finnigan Triton T1 thermal ionization mass spectrometer (TIMS) at the Helmholtz-Zentrum für Ozeanforschung Kiel, GEOMAR, closely following the method and use of standards described by Heuser et al. (2002). Tantalum chloride ($TaCl_5$) was used as activator to enhance Ca ionization efficiency. An in-house calcium fluorite (CaF_2) standard was included to monitor accuracy. Sample and standard $\delta^{44/40}$Ca values are referenced to the standard SRM 915a. External reproducibility assessed by repeatedly measuring CaF_2 was 0.17‰ (2σ, $n = 33$) and an average isotopic value of 1.45‰ was calculated, which is in the range of the mean CaF_2 isotopic value reported by Heuser et al. (2002) for multicup measurements

Table 1
Biomass, Ca consumption, $CO_{2\,aq}$, Ca isotopic fractionation ($\Delta^{44/40}Ca_{cocco\text{-}sw}$), C isotopic fractionation ($\varepsilon_{coccolith}$), calcification rate normalized to surface area (SA) and Sr/Ca from culture experiments with varying ambient CO_2 and DIC. The precision of $\Delta^{44/40}Ca_{cocco\text{-}sw}$ is reported as $2\sigma/n^{0.5}$ of the $\delta^{44/40}Ca$ measurements. n refers to the number of $\delta^{44/40}Ca$ measurements per sample to achieve $2\sigma/n^{0.5} \leq 0.10$. Due to high Ca blanks, calcification rate/SA and Ca consumption could not be calculated for *C. leptoporus*.

		Biomass (µg POC/mL)	Ca consumption (%)	$CO_{2\,aq}$ (mmol/kg)	$\Delta^{44/40}Ca_{cocco\text{-}sw}$ (‰)	n	$\varepsilon_{coccolith}$ (‰)	Calcification rate/SA (pg C/(µm^2 day))	Sr/Ca (mmol/mol)
E. huxleyi	$[CO_2]$	1.51	0.17	5.4	−1.41 ± 0.09	12	1.57	0.10	2.92
		0.33	0.04	31.9	−1.19 ± 0.08	8	2.06	0.06	2.84
		0.61	0.01	58.3	−1.06 ± 0.08	5	3.39	0.02	2.65
	DIC	0.63	0.04	8.8	−1.46 ± 0.10	8	2.24	0.08	3.23
		0.68	0.05	12.4	−1.27 ± 0.07	17	1.49	0.09	3.11
		0.60	0.07	17.2	−1.56 ± 0.05	3	2.15	0.12	3.23
C. leptoporus	$[CO_2]$	0.61		5.9	−1.50 ± 0.07	3	−2.84		2.15
		0.85		36.1	−1.34 ± 0.03	3	−0.63		2.66
		0.79		56.9	−1.38 ± 0.08	3	0.32		3.11
G. oceanica	$[CO_2]$	0.42	0.03	6.6	−1.31 ± 0.07	8	2.27	0.10	2.80
		0.56	0.02	27.3	−1.36 ± 0.10	3	3.38	0.05	2.95
		0.47	0.01	66.8	−1.24 ± 0.09	3	2.46	0.04	2.71

Table 2
Correlation of Ca isotopic fractionation ($\Delta^{44/40}Ca_{cocco\text{-}sw}$) with CO_2 concentrations, C isotopic fractionation ($\varepsilon_{coccolith}$), calcification rate normalized to SA and Sr/Ca and significance levels (in parenthesis) from culture experiments with varying CO_2 and DIC. $n = 3$ except when indicated by $*$, where $n = 6$. Correlations are linear except when indicated by italics (logarithmic). Bold characters indicate significant relationships ($p < 0.1$).

	E. huxleyi			*C. leptoporus*	*G. oceanica*
	$[CO_2]$	DIC	$[CO_2]$ + DIC	$[CO_2]$	$[CO_2]$
	$\Delta^{44/40}Ca_{cocco\text{-}sw}$	$\Delta^{44/40}Ca_{cocco\text{-}sw}$	$\Delta^{44/40}Ca_{cocco\text{-}sw}$	$\Delta^{44/40}Ca_{cocco\text{-}sw}$	$\Delta^{44/40}Ca_{cocco\text{-}sw}$
$[CO_2]$ (µmol/kg)	0.991 **(0.086)**	−0.407 (0.733)	0.795 **(0.059)***	*0.917 (0.262)*	0.717 (0.491)
$\varepsilon_{coccolith}$ (‰)	*0.954 (0.194)*	−0.901 (0.286)	0.497 (0.316)*	*0.949 (0.205)*	−0.710 (0.497)
Calcification rate/SA (pg C/(cell day µm^2))	−0.987 (0.104)	−0.497 (0.669)	−0.873 **(0.023)***		−0.249 (0.840)
Sr/Ca (mmol/mol)	−0.937 (0.227)	−0.925 (0.249)	−0.860 **(0.028)***	*0.792 (0.418)*	−0.970 (0.157)

(1.43‰). The precision of sample $\delta^{44/40}Ca$ measurements was reported as the standard deviation of the mean ($2\sigma_{mean} = 2\sigma/n^{0.5}$) and was better than 0.1‰ (Table 1). Sample Ca blank content varied between ∼8 and ∼15 ng, remaining <5% of the total Ca in samples. Blank $\delta^{44/40}Ca$ values (0.78–1.51‰) remained in the range of isotopic values measured for samples and standards. Due to the similar blank $\delta^{44/40}Ca$ and the very low blank content in samples, we do not expect blank contribution to have significantly affected results and we do not employ blank corrections.

2.4. Calculations

Ca isotopic fractionation between the calcite of cultured coccolithophores and the media ($\Delta^{44/40}Ca_{cocco\text{-}sw}$) was reported as the difference between coccolith and seawater Ca isotopic composition: ($\delta^{44/40}Ca_{coccolith} - \delta^{44/40}Ca_{seawater}$). $\delta^{44/40}Ca_{coccolith}$ is more negative than $\delta^{44/40}Ca_{seawater}$, so increased fractionation and deviation from the $\delta^{44/40}Ca_{seawater}$ value is reflected by more negative $\Delta^{44/40}Ca_{cocco\text{-}sw}$ values. Since nutrients added to natural seawater contain no Ca or Sr, and none of the methods used during culture are expected to have modified the original $\delta^{44/40}Ca_{seawater}$, and since Ca depletion during culturing remained <0.2%, we do not expect culture experiments to have significantly affected the original $\delta^{44/40}Ca_{seawater}$ value. Therefore, we assume seawater $\delta^{44/40}Ca$ values for our calculations to be 1.9‰, which is the median value of modern seawater measured by TIMS (Fantle and Tipper, 2014).

3. Results

3.1. Coccolith $\delta^{44/40}Ca$, $\delta^{13}C$ and Sr/Ca

The $\Delta^{44/40}Ca_{cocco\text{-}sw}$ of cultured coccoliths varied between −1.56 and −1.06‰ (Table 1), a range comparable to previous determinations of cultured coccoliths and other marine biogenic carbonates (e.g. De la Rocha and DePaolo, 2000; Gussone et al., 2007, 2006; Langer et al., 2007; Kısakürek et al., 2011; Müller et al., 2011). For *E. huxleyi*, in all experiments, higher calcification rates lead to more negative $\Delta^{44/40}Ca_{cocco\text{-}sw}$ (Fig. 1a, Table 2). The positive correlation observed between $\Delta^{44/40}Ca_{cocco\text{-}sw}$ and CO_2 for *E. huxleyi* (Fig. 1b, Table 2) can be explained by the inverse correlation between CO_2 and calcification rate ($r = -0.87$; $p = 0.02$; $n = 6$; Fig. 1e).

On the other hand, for *G. oceanica*, $\Delta^{44/40}Ca_{cocco\text{-}sw}$ does not correlate significantly with calcification rate. Also, the correlation between calcification rate and seawater CO_2 is insignificant for *G. oceanica* ($r = 0.85$; $p = 0.35$; $n = 3$) and $\Delta^{44/40}Ca_{cocco\text{-}sw}$ does not correlate with seawater CO_2 (Fig. 1b, Table 2). The lack of reliable PIC measurements for *C. leptoporus* hinders accessing the relationship between $\Delta^{44/40}Ca_{cocco\text{-}sw}$ and calcification rate for this species.

Higher HCO_3^- allocation to calcification under non-limiting CO_2 conditions is expressed in the carbon isotopic fractionation of coccoliths by a higher $\varepsilon_{coccolith}$ (Bolton and Stoll, 2013). As expected, $\varepsilon_{coccolith}$ and seawater CO_2 were directly correlated for both *C. leptoporus* ($r = 0.99$; $p = 0.08$; $n = 3$) and for *E. huxleyi* ($r = 0.87$; $p = 0.03$; $n = 6$). In the case of *G. oceanica*, no correlation between CO_2 and $\varepsilon_{coccolith}$ was observed ($r = 0.02$; $p = 0.99$; $n = 3$) (Fig. 1d). The lowest $\varepsilon_{coccolith}$ values at low seawater CO_2 are found for the coccoliths of the larger *C. leptoporus* (Fig. 1d, Table 1), which is consistent with previous models (Bolton and Stoll, 2013). The modest direct logarithmic correlations between $\varepsilon_{coccolith}$ and $\Delta^{44/40}Ca_{cocco\text{-}sw}$ for the CO_2 experiments of *E. huxleyi* and *C. leptoporus* (Fig. 1c, Table 2) could indicate a potential link between carbon and calcium cellular regulation in coccolithohores. Similarly, the negative correlation between $\Delta^{44/40}Ca_{cocco\text{-}sw}$ and Sr/Ca for *E. huxleyi* and *G. oceanica* shows a potential link between Sr and Ca cellular pathways. Conversely, an insignificant direct correlation was observed for $\Delta^{44/40}Ca_{cocco\text{-}sw}$ and Sr/Ca in *C. leptoporus* (Fig. 1f, Table 2).

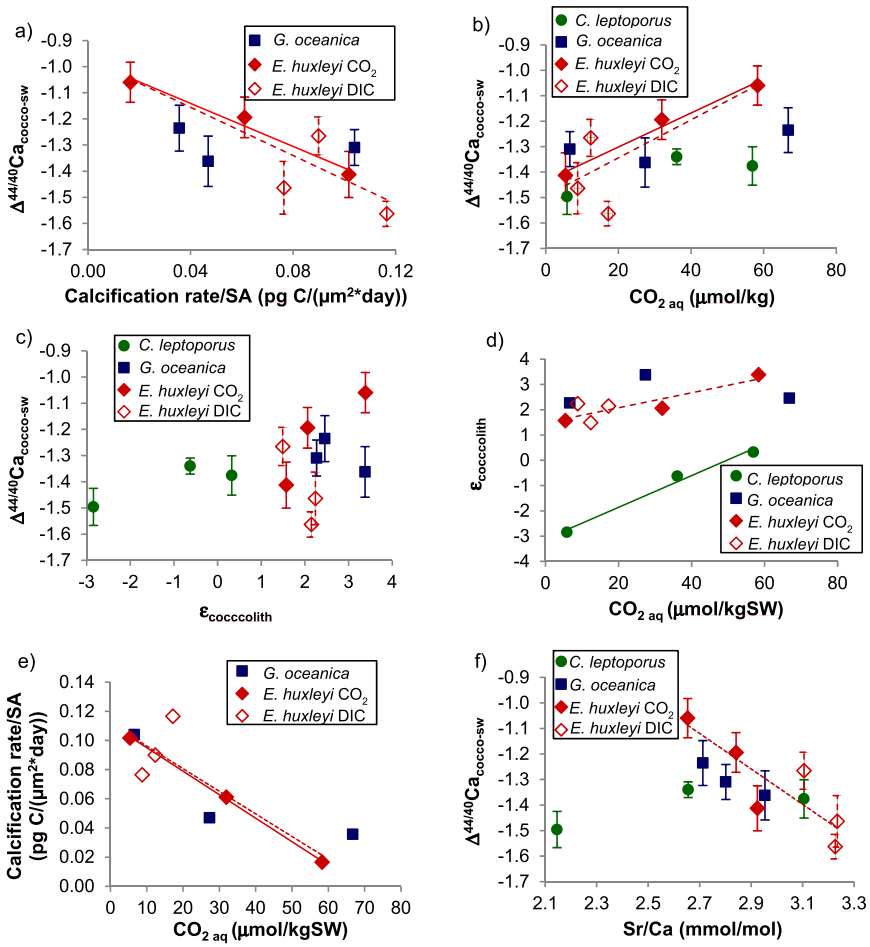

Fig. 1. Ca isotopic fractionation ($\Delta^{44/40}Ca_{cocco\text{-}sw}$ (‰)) as a function of a) calcification rate normalized to SA (pg C/(µm^2∗day)), b) media CO_2 concentrations (µmol/kg), c) C isotopic fractionation ($\varepsilon_{coccolith}$ (‰)). d) $\varepsilon_{coccolith}$ as a function of media CO_2 concentrations, e) calcification rate/SA as a function of media CO_2 concentrations, f) $\Delta^{44/40}Ca_{cocco\text{-}sw}$ as a function of coccolith Sr/Ca (mmol/mol) from culture experiments with varying ambient CO_2 of *C. leptoporus*, *G. oceanica* and *E. huxleyi*, and varying DIC of *E. huxleyi*. Linear regressions of statistically significant ($p < 0.1$) correlations are shown as solid (varying CO_2 experiments) and dashed (varying CO_2 and DIC experiments) lines. Significance levels of the correlations are given in Table 2 and the main text in section 3.1.

4. Model of Ca isotopic fractionation in coccolithophores

4.1. Biological context and basis of the model

Here we propose a simple cellular model of coccolith Ca isotopic fractionation and Sr/Ca (named CaSri–Co). The model shows that given fractionation during desolvation, variation in calcification rate, the efficiency at which Ca that is taken up is fixed into calcite, and the characteristics of the solvation environment, could explain a large part of coccolith Ca isotopic fractionation and Sr/Ca variability. This is the simplest model that incorporates current knowledge of processes of cellular Ca and Sr transport, though there may be additional processes involved yet to be described.

4.1.1. Ca and Sr uptake and transport within the cell

Previous studies have shown that Ca ions from seawater ([Ca] = ~10 mM) enter the cytosol through the plasma membrane (PM) (F_{in}) via Ca permeable channels, following an electrochemical potential gradient (Mackinder et al., 2011, 2010) (Fig. 2a). Coccolithophores must maintain low and stable (~0.1 µM) cytosolic Ca concentrations (Brownlee et al., 1995) because several important cell processes and signaling systems are controlled by localized and reversible changes in Ca concentrations (Mackinder et al., 2010). Therefore, excess Ca must be efficiently removed from the cytosol.

After crossing the plasma membrane (F_{in}), Ca is either used for calcification (F_{ER}) or transported back to seawater (F_{OUT}), possibly actively via Ca^{2+}-ATPases (Mackinder et al., 2011). F_{in}, F_{ER} and F_{OUT} therefore refer to Ca ion fluxes between seawater and different cell compartments. Ca that is used for calcification is thought to be transported to the endoplasmic reticulum/reticular body and its endomembrane system (ER), likely through Ca^{2+}/H^+ exchangers such as VCX/CAX-like proteins (Mackinder et al., 2011). This Ca uptake may occur mainly near the cytosolic microenvironment (CM) formed by the proximity of the endoplasmic reticulum membrane and the plasma membrane (Berry et al., 2002). This would avoid the remaining cytosol reaching high Ca concentrations while allowing favorable conditions for Ca uptake through the endoplasmic reticulum membrane. The Ca that enters the endoplasmic reticulum is subsequently transported to the coccolith vesicle (CV) for calcification (Mackinder et al., 2010) (Fig. 2a, Fig. 4a).

Sr probably shares the same transport mechanisms as Ca (Müller et al., 2011). Therefore, we assume that the transport of Sr depends on the same factors as those controlling Ca transmembrane passage. A critical difference is that all the Ca transported to the endoplasmic reticulum and the coccolith vesicle is assumed to be fixed in calcite (Gussone et al., 2006), whereas the low partition coefficient of Sr in calcite produces a residual Sr content in the coccolith vesicle. This residual Sr is assumed to be transported back to the cytosolic microenvironment (Fig. 2a, Fig. 4b).

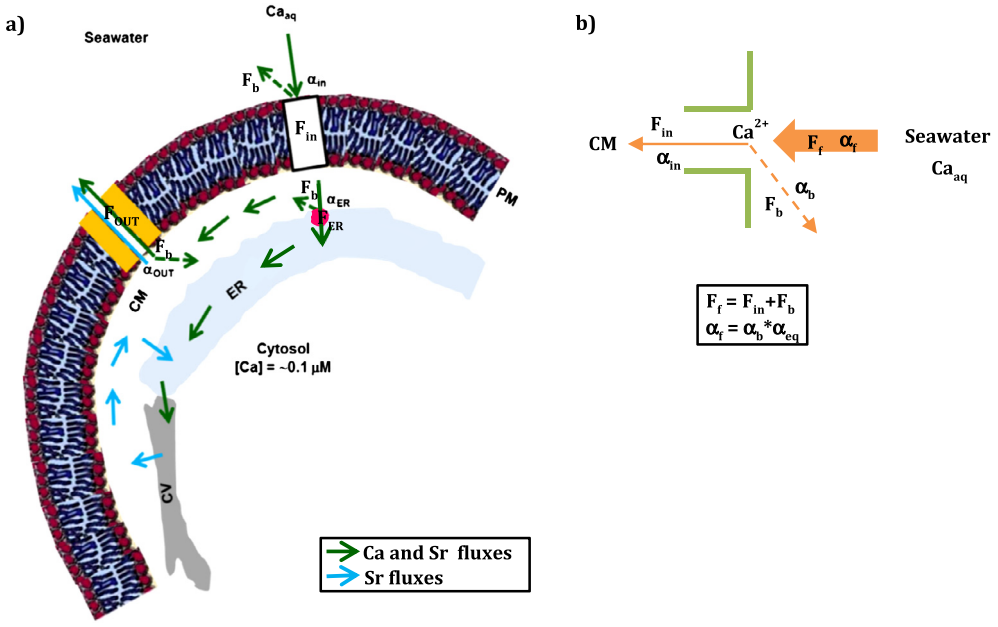

Fig. 2. a) Schematics of the cellular Ca and Sr pathways considered for the CaSri–Co model of coccolith Ca isotopic fractionation and Sr/Ca ratios (Mackinder et al., 2011, 2010). Ca is taken up from seawater into the cytosolic microenvironment (CM) (F_{in}) via Ca permeable channels in the plasma membrane (PM) (white rectangle). Ca uptake from the cytosolic microenvironment to the endoplasmic reticulum (ER) (F_{ER}) may occur through Ca^{2+}/H^{+} exchangers in the endoplasmic reticulum membrane (pink circle). The excess of Ca inside the cytosolic microenvironment is thought to be transported back to seawater (F_{OUT}) via Ca ATPases (double yellow rectangles), which appear to be involved in Ca homeostasis. Ca and Sr are assumed to share the same pathways (green solid arrows). Light blue arrows represent the Sr pathways assumed during calcification. The fraction of Sr that is not incorporated into calcite is assumed to be transported back to the cytosolic microenvironment. b) Example of fluxes and fractionation factors during transport across Ca channels. A flux of hydrated Ca ions (Ca_{aq}) in seawater are desolvated/dehydrated (F_f) and enter the reservoir at the docking site of the Ca channel (Ca^{2+}). Desolvation has an associated fractionation factor (α_f). Part of these desolvated Ca ions are transported across the channel (F_{in}) to the cytosolic microenvironment, and part of them are resolvated/rehydrated and return to seawater (F_b: dashed arrows) ($F_f = F_{in} + F_b$), with an associated fractionation factor (α_b) that depends on α_f and α_{eq} ($\alpha_f = \alpha_b * \alpha_{eq}$). The effective fractionation associated with each transmembrane passage (α_{in}, α_{ER}, and α_{OUT}) depends on these fluxes and on the fractionation factors associated with them. This process also describes fluxes and fractionation factors during the other considered transmembrane transport steps and coccolith precipitation. For the later case, membrane transporters, F_b and F_{in} in this example are analogous to the calcite crystal, dissolution rate and precipitation rate, respectively. Coccolith $\delta^{44/40}Ca$ are not affected by desolvation–solvation during coccolith precipitation because all the Ca taken up by the endoplasmic reticulum is assumed to ultimately be fixed into calcite. (For interpretation of the references to color in this figure legend, the reader is referred to the web version of this article.)

Due to the high Ca concentration and flux requirements for fast calcification of single coccoliths (Gussone et al., 2006; Holtz et al., 2013), it is very likely that Ca transported to the endoplasmic reticulum is entirely used for calcification in the coccolith vesicle (Gussone et al., 2006). For complete Ca consumption, enough carbon needs to be available in the coccolith vesicle for calcification, which would imply coupling between the Ca and C systems in coccolithophores. This might be by regulation of Ca uptake by the endoplasmic reticulum. It might also occur by regulation of the carbon supply or carbon speciation in the coccolith vesicle, for instance, by regulating active bicarbonate transport to the coccolith vesicle (Bolton and Stoll, 2013).

We assume a complete consumption of the Ca taken up by the endoplasmic reticulum. Therefore, the calcification rate calculated from culture studies must equal the net Ca flux to the endoplasmic reticulum and the net flux to the coccolith vesicle (F_{ER}). However, there is no independent constraint on cellular Ca uptake through the plasma membrane (F_{in}). F_{in} must be at least equal to F_{ER} (i.e. 100% of Ca taken up is used for calcification), but the cellular Ca influx (F_{in}) could be in excess of the Ca used for calcification (F_{ER}), implying a lower Ca retention efficiency (F_{ER}/F_{in}) and higher Ca outflow to seawater (F_{OUT}) (Appendix A).

Coccolithophores are expected to be able to regulate Ca retention efficiency to maintain low cytosolic Ca (Brownlee et al., 1995) while using Ca channels as the main Ca uptake mechanism (Mackinder et al., 2011, 2010). The Ca flux across the Ca channels cannot be closely regulated by cells, as opposed to Ca flux across other active transporters (e.g. Ca^{2+}-ATPases or Ca^{2+}/H^{+} exchangers) (Brownlee, pers. comm.). Therefore, it is feasible that the cell permits Ca channels to operate at some excess, and maintain low cytosolic Ca concentrations by a fine regulation of the transport back to seawater of the unused Ca contained in the cytosolic microenvironment. This is consistent with the hypothesis of the study of Müller et al. (2015), who have suggested that Ca enters in excess to the cell and calcification may have evolved as a mechanism of cellular detoxification in coccolithophores. The ability to regulate Ca retention efficiency would allow coccolithophores to also control the amount of Ca taken up by the endoplasmic reticulum and balance the carbon available for calcification, implying a potential coupling between their Ca and C systems. Further studies are required to confirm this link.

The CaSri–Co model was built as a steady-state model, based on the observation that continuous fluxes of Ca between reservoirs are required to achieve a continuous and rapid (1 h for *E. huxleyi*) coccolith calcification (Gussone et al., 2006; Holtz et al., 2013). Given the volumes, surface areas and Ca concentrations reported in the literature for *E. huxleyi* (Gussone et al., 2006; Holtz et al., 2015, 2013) and our average Ca fluxes, a maximum total time of ~4.1 s is required for the initial filling of the cytosolic microenvironment, endoplasmic reticulum and coccolith vesicle compartments with Ca (Appendix B). Similarly, the final phase of construction of the coccolith, where Ca is consumed but not renewed and hence not in steady-state, is estimated at ~4.2 s, given the increased volume and surface area of the coccolith vesicle at that time. Thus, out of the total time of coccolith formation (3600 s), only a negligible portion (~8.3 s) occurs under transient conditions, while the rest of the time (3591.7 s) occurs in steady-state conditions. The composition of the coccolith is thus dominated by the steady-state operation of time-independent Ca transport rates and constant Ca concentrations/isotopic compositions within in-

tracellular reservoirs. Therefore, the steady-state approach of our model is expected to adequately simulate the coccolith Ca isotopic composition (Appendix B).

Our model contemplates Ca transport to the coccolith vesicle from the cytosolic microenvironment exclusively via the endoplasmic reticulum (Fig. 2a). However, specific intracellular Ca pathways in coccolithophores have not yet been resolved and there are ongoing discussions and different hypotheses which postulate how Ca may be actually transported from the site of uptake to the coccolith vesicle (Holtz et al., 2013). Recent modeling studies have proposed that Ca transport in *E. huxleyi* may occur directly from the cytosol to the coccolith vesicle potentially via Ca^{2+}/H^{+} antiport or Ca^{2+} and HCO_3^- import and H^+ export (Holtz et al., 2013), although kinetic considerations make cytosolic diffusive Ca transport to the coccolith vesicle less likely (Brownlee and Taylor, 2005). Given that in our model all of the Ca taken up by the endoplasmic reticulum is ultimately fixed in the coccolith vesicle, our model would also apply to a direct Ca uptake by the coccolith vesicle, as the number of steps where Ca isotopic fractionation occurs would remain unaltered.

4.1.2. Coccolith Ca isotopic fractionation

Fractionation in the model is based on the assumption that Ca desolvation–solvation before and during Ca transmembrane transport constitute the sole mechanism responsible for Ca isotopic fractionation. This assumption was originally suggested by Gussone et al. (2006). Model studies have also suggested Ca isotopic fractionation to be caused by Ca desolvation/dehydration (i.e. removal of water – solvent – from Ca – solute: Ca aqua complex (Ca_{aq}) → Ca ions (Ca^{2+})) during precipitation of calcite in aqueous solutions (DePaolo, 2011; Hofmann et al., 2012). The kinetics of desolvation during Ca transport favors the light isotope (Gussone et al., 2003; Hofmann et al., 2012). Our assumption that desolvation–solvation dynamics are also determinant for the more complex biologically-controlled systems (i.e. coccoliths), as it is for abiotic calcite precipitation, finds support in studies of molecule transmembrane transport (e.g. Burton et al., 1992; Conradi et al., 1991). These studies have revealed that molecule desolvation is required for both active and passive transport across membranes of epithelial cells. Moreover, desolvation has been found to play key roles in other biological-driven processes such as enzyme catalysis reactions (e.g. Klibanov, 2001; Wescott et al., 1996). The widely extended importance of desolvation in biology indicates that its influence on Ca isotopic fractionation is not limited to abiotic systems, but is also a key process for biological systems.

Apart from Ca desolvation–solvation dynamics, further mechanisms not contemplated in this model because their potential effects in biological systems are largely unknown, may also play a role in controlling Ca isotopic fractionation in coccolithophores. For instance, the expected faster diffusion rate of the lighter ^{40}Ca compared to the heavier ^{44}Ca *inside* transporters could potentially contribute to Ca isotopic fractionation. If this were true, the fractionation factor associated with diffusion would be expected to be <1 (Fantle and DePaolo, 2007). Fractionation during diffusion of Ca isotopes in aqueous solutions on the order of $-0.4‰$ was observed by Bourg et al. (2010). On the other hand, ion diffusion in seawater at the site of uptake is not expected to contribute to Ca isotopic fractionation under our well-mixed culture conditions. This is because of the low dependence of the Ca diffusion coefficient on its mass (Bourg et al., 2010) and the high seawater Ca concentration (10 mM) relative to uptake rates in coccolithophores (7×10^{-9}–2.3×10^{-5} mol/m^2/s; estimates from this study), and relative to experimental abiogenic precipitation rates (e.g. 7.2×10^{-11}–1.8×10^{-10} mol/m^2/s from Tang et al., 2008). In addition to diffusion inside transporters, Ca is also suggested to fractionate during adsorption/desorption reactions (Fantle et al., 2012) and calcite recrystallization at low precipitation rates (Fantle and DePaolo, 2007). Determining whether the influence of such mechanisms is significant or not in driving Ca isotopic fractionation in biologically-driven systems like that of coccolithophores, requires further study and is outside the scope of this work.

Here we simulate three transmembrane transport steps where desolvation causes Ca isotopic fractionation. These include: a) from the seawater reservoir into the cytosolic microenvironment reservoir across the plasma membrane (α_{in}); b) from the cytosolic microenvironment to the endoplasmic reticulum reservoir across the endoplasmic reticulum membrane (α_{ER}); and c) from the cytosolic microenvironment back into seawater across the plasma membrane (α_{OUT}) (Fig. 2a; Fig. 4a). The model describes the effective fractionation associated with each of these three transmembrane transport steps (α_{in}, α_{ER}, α_{OUT}) as resulting from: a) the forward (F_f) and reverse (F_b) reaction rates of desolvation and solvation, respectively; b) the maximum fractionation of desolvation between the hydrated Ca (Ca_{aq}) and dehydrated Ca (Ca^{2+}) (α_f); and c) the equilibrium fractionation factor between Ca_{aq} and Ca^{2+} (α_{eq}). α_{eq} depends on the microenvironment at the docking site of transporters (Eqs. (1a), (1b), (1c)).

The forward reaction rate (desolvation, F_f) is the flux of Ca that is dehydrated before a specific transmembrane transport occurs. The reverse reaction rate (solvation, F_b) describes the part of the Ca forward flux that is rehydrated at the docking site of the specific transmembrane transporter and is returned to the previous reservoir (i.e. seawater or CM). Both desolvation (F_f) and solvation (F_b) have an associated fractionation factor (α_f and α_b, respectively; $\alpha_f = \alpha_b * \alpha_{eq}$) (Fig. 2b). In our model construction, coccolithophores are precipitating coccoliths, and therefore F_f must be $> F_b$ for the Ca transport steps from seawater to the cytosolic microenvironment and from the cytosolic microenvironment to the endoplasmic reticulum, so there is net Ca supplied for calcification. An equilibrium condition ($F_f = F_b$) can only be met in our model construction at the transport step from the cytosolic microenvironment to seawater if Ca retention efficiency (F_{ER}/F_{in}) was 100%, wherewith there would not be a net forward Ca transport back to seawater ($F_{OUT} = 0$).

Our model formulation is analogous to the surface kinetic model described by DePaolo (2011) for calcite precipitation from aqueous solutions, and similar to that originally applied by Fantle and DePaolo (2007) to model the results of Lemarchand et al. (2004) and those from their sediments at Site 807A. Fantle and DePaolo (2007) suggested that similar mechanisms may be driving Ca isotopic fractionation of inorganic calcite precipitation and biologically-driven calcite formation. A parallel treatment of the transmembrane Ca transport system in coccolithophores is possible because the dynamics of Ca desolvation and posterior attachment to the crystal surface parallels that of Ca desolvation prior to Ca transmembrane passage and posterior attachment to for instance, a protein transporter in the membrane. Similar thermodynamics between these two systems were already suggested by Gussone et al. (2006). The relevant equations for individual effective fractionations are:

$$\alpha_{in} = \frac{\left(\frac{^{44}Ca}{^{40}Ca}\right)_{CM}}{\left(\frac{^{44}Ca}{^{40}Ca}\right)_{SW}} = \frac{\alpha_f}{1 + \frac{F_b}{F_{in}+F_b}\left(\frac{\alpha_f}{\alpha_{eq}} - 1\right)} \tag{1a}$$

$$\alpha_{ER} = \frac{\left(\frac{^{44}Ca}{^{40}Ca}\right)_{ER}}{\left(\frac{^{44}Ca}{^{40}Ca}\right)_{CM}} = \frac{\alpha_f}{1 + \frac{F_b}{F_{ER}+F_b}\left(\frac{\alpha_f}{\alpha_{eq}} - 1\right)} \tag{1b}$$

$$\alpha_{OUT} = \frac{\left(\frac{^{44}Ca}{^{40}Ca}\right)_{SW}}{\left(\frac{^{44}Ca}{^{40}Ca}\right)_{CM}} = \frac{\alpha_f}{1 + \frac{F_b}{F_{OUT}+F_b}\left(\frac{\alpha_f}{\alpha_{eq}} - 1\right)} \tag{1c}$$

The effective fractionation during transmembrane transport (α_{in}, α_{ER}, α_{OUT}) is maximized when the forward reaction rate is greater than the reverse reaction rate (highest ratio of F_f/F_b) (DePaolo, 2011). The forward (desolvation) rate (F_f) at each of the three transmembrane transport steps can be calculated from the modeled net Ca flux across a given membrane (F_{in}, F_{ER}, F_{OUT}) and the backwards flux (F_b), such that $F_f = F_b + F_{in}$ or F_{ER} or F_{OUT} (Fig. 2b). Unfortunately, there is little information available to theoretically constrain the magnitude of F_b (solvation rate), which, in addition to the solvation environment properties, may also vary depending on specific membrane constituents. More hydrocarbon-like membranes with less hydrogen-bonding potential tend to face higher desolvation energies, complicating solute transmembrane transport (Conradi et al., 1991), and potentially also influencing F_b. The magnitude of the effective fractionation associated with each transmembrane passage (α_{in}, α_{ER}, α_{OUT}) is constrained between the maximum fractionation of desolvation (α_f) and the equilibrium fractionation factor (α_{eq}).

Given the theoretical uncertainties of the magnitudes of F_b and α_f, we chose their values based on consistency of modeled coccolith Ca isotopic fractionation ($\Delta^{44/40}Ca_{cocco\text{-}sw}$) with the observed data from our cultures and those of *E. huxleyi* of the studies of Gussone et al. (2006), Langer et al. (2007) and Müller et al. (2011). For the simplest version of the model, we assume uniform F_b and α_f magnitudes for the different transmembrane passages considered (Fig. 5; Appendix A). Modeled $\Delta^{44/40}Ca_{cocco\text{-}sw}$ are most consistent with the observed data when an α_f of 0.9982 (−1.802‰) and an F_b of 5×10^{-8} mol/m^2/s are used. The chosen α_f is within the range of α_f values reported by Hofmann et al. (2012) for infinite dilutions (0.9953; −4.7‰). The choice of F_b modulates the slope of the $\Delta^{44/40}Ca_{cocco\text{-}sw}$ dependence on calcification (Fig. 5b; section 4.2), while the choice of α_f modulates the absolute magnitude of coccolith $\Delta^{44/40}Ca_{cocco\text{-}sw}$ (Fig. 3).

On the other hand, the equilibrium fractionation factor (α_{eq}) depends on the specific microenvironment at the docking site of transporters. For the simplest version of our model, we assume a homogeneous α_{eq} of 1. This is the value for fractionation at equilibrium (balanced dissolution and precipitation) found by Fantle and DePaolo (2007) for very slow calcite precipitation rates, and is the same as used in DePaolo (2011). An $\alpha_{eq} = 1$ implies no preference for the light isotope by transporters, and assumes the same fractionation factor associated with desolvation (α_f) and solvation (α_b) fluxes (since $\alpha_f = \alpha_b * \alpha_{eq}$) (Fig. 2b). However, we note that fractionation at equilibrium may not necessarily be the same for Ca transport across membrane transporters as it is for calcite precipitation. Furthermore, since the microenvironment at the docking site of Ca^{2+}/H^+ exchangers and Ca ATPases may be different from that at the entrance of Ca channels, as only the last type of transporter works following an electrochemical gradient, there may be potential differences in α_{eq} associated with the different transport steps here considered. The F_b magnitude could also differ between transport via pumps and Ca channels due to the different characteristics of the cytosolic microenvironment and seawater. Since there is potential for α_{eq} and F_b to vary amongst intern transport and transport across Ca channels, model results using constant (Fig. 5) and variable values of α_{eq} and F_b are shown as a sensitivity analysis in Appendix C.

For our steady state model the Ca fluxes into (F_{in}) and out (F_{ER} and F_{OUT}) of the cytosolic microenvironment and their respective $\delta^{44/40}Ca$ (δ_{in}, δ_{ER}, δ_{OUT}) are equal (mass balance equation: Eq. (2); Fig. 4a). The isotopic composition of the desolvated Ca that is transported successfully through each membrane (δ_{in}, δ_{ER}, δ_{OUT}) depends on the Ca isotopic composition of the reservoir from which it is removed (seawater – δ_{sw} – or cytosolic microenvironment – δ_{CM}), and the effective fractionation associated with this specific transmembrane transport step (α_{in}, α_{ER}, α_{OUT}) (Eqs. (3a), (3b), (3c)). The Ca isotopic composition of the cytosolic microenvironment (δ_{CM}) is mathematically resolved by substituting the δ_{ER} and δ_{OUT} terms of the mass balance equation (Eq. (2)) with the equations (3b) and (3c), and solving for δ_{CM}. Because Ca isotopic fractionation occurs at the three considered transport steps (seawater to cytosolic microenvironment, cytosolic microenvironment to endoplasmic reticulum and cytosolic microenvironment to seawater), the $\delta^{44/40}Ca$ of the cytosolic microenvironment reservoir (δ_{CM}) is affected by the effective fractionation (α_{in}, α_{ER}, α_{OUT}) and by the Ca fluxes (F_{in}, F_{ER}, F_{OUT}) associated with individual Ca passages, and by factors influencing them (Eq. (3d)). Consequently, in our model there is a successive evolution of the $\delta^{44/40}Ca$ from seawater compared to that of the endoplasmic reticulum. A complete consumption of the Ca taken up by the endoplasmic reticulum implies no further net fractionation between the endoplasmic reticulum and the coccolith vesicle or coccolith calcite and that the Ca isotopic composition measured in the coccolith (δ_{cocco}) is equivalent to that of Ca entering the endoplasmic reticulum (δ_{ER}) (Fig. 4a). The relevant equations are:

$$F_{in} * \delta_{in} = F_{ER} * \delta_{ER} + F_{OUT} * \delta_{OUT} \quad (2)$$

$$\delta_{in} = \delta_{SW} + 1000 \ln \alpha_{in} \quad (3a)$$

$$\delta_{ER} = \delta_{CM} + 1000 \ln \alpha_{ER} \quad (3b)$$

$$\delta_{OUT} = \delta_{CM} + 1000 \ln \alpha_{OUT} \quad (3c)$$

$$\delta_{CM} = \frac{\delta_{in} * F_{in} - 1000 \ln \alpha_{ER} * F_{ER} - 1000 \ln \alpha_{OUT} * F_{OUT}}{F_{ER} + F_{OUT}} \quad (3d)$$

Contrary to the variable cytosolic microenvironment reservoir, here we assume that the $\delta^{44/40}Ca$ of the seawater infinite reservoir (boundary condition) is constant ($\delta_{sw} = 1.9$‰) (Appendix A), given our assumption that ion diffusion in seawater should not affect coccolith Ca isotopic fractionation under well-stirred conditions (i.e. our cultures and natural-growing populations). However, as suggested by previous authors (e.g. Tang et al., 2008), we acknowledge a potential effect of ion diffusion in the seawater solvation environment under unstirred conditions. In this way, the formation of a boundary layer enriched in the heavier ^{44}Ca due to diffusive limitations could produce coccoliths with comparatively higher Ca isotopic compositions. This would be most evident in cultures of larger coccolithophores grown under unstirred conditions, potentially explaining the overall heavier isotopes observed in the study

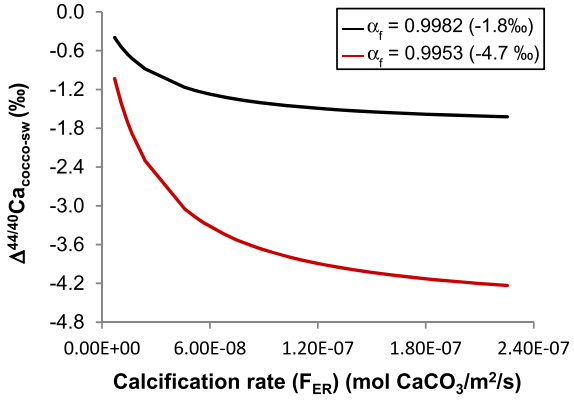

Fig. 3. Modeled coccolith Ca isotopic fractionation ($\Delta^{44/40}Ca_{cocco\text{-}sw}$ (‰)) as a function of calcification rate normalized to surface area (F_{ER} (mol $CaCO_3$/m^2/s) at a constant Ca retention efficiency (F_{ER}/F_{in}) of 50%, constant F_b of 5×10^{-8} mol/m^2/s, and using two different values of maximum fractionation of desolvation: α_f = 0.9982 (−1.8‰), as used here to model cultured coccolithophores (black); α_f = 0.9953 (−4.7‰), as estimated for infinite dilutions (Hofmann et al., 2012) (red)). (For interpretation of the references to color in this figure legend, the reader is referred to the web version of this article.)

of Müller et al. (2011) for the larger *Coccolithus braarudii*, compared to our cultures and to other *E. huxleyi* cultures discussed in section 4.2.

4.1.3. Coccolith Sr/Ca

The CaSri–Co model also tracks cellular Sr uptake and transport, and coccolith Sr/Ca. Sr and Ca are thought to share cellular transport mechanisms, pathways and transporters (Müller et al., 2011) (Fig. 2a). Consequently, the similarity between Ca isotopic fractionation and Sr/Ca partitioning suggested for abiotic calcite precipitation from aqueous solutions (DePaolo, 2011) should also apply to transmembrane Sr/Ca transport. Therefore, we calculate the effective Sr/Ca partitioning associated with the three transmembrane transport steps ($K_{\text{f-in}}$: from seawater to the cytosolic microenvironment; $K_{\text{f-ER}}$: from the cytosolic microenvironment to the endoplasmic reticulum; $K_{\text{f-OUT}}$: from the cytosolic microenvironment to seawater) (Eqs. (4a), (4b), (4c)) as α_{in}, α_{ER} and α_{OUT} were calculated (section 4.1.2). $K_{\text{f-in}}$, $K_{\text{f-ER}}$ and $K_{\text{f-OUT}}$ result from the desolvation ($F_{\text{f}} = F_{\text{b}} + F_{\text{in}}$ or F_{ER} or F_{OUT}) and solvation (F_{b}) reaction rates of Ca (and of Sr transported by Ca transporters), the forward kinetic partition coefficient for Sr/Ca (K_{f}), and the equilibrium Sr/Ca partition coefficient (K_{eq}). The relevant equations are:

$$K_{\text{f-in}} = \frac{\left(\frac{\text{Sr}}{\text{Ca}}\right)_{\text{CM}}}{\left(\frac{\text{Sr}}{\text{Ca}}\right)_{\text{SW}}} = \frac{K_{\text{f}}}{1 + \frac{F_{\text{b}}}{F_{\text{in}}+F_{\text{b}}}\left(\frac{K_{\text{f}}}{K_{\text{eq}}} - 1\right)} \tag{4a}$$

$$K_{\text{f-ER}} = \frac{\left(\frac{\text{Sr}}{\text{Ca}}\right)_{\text{ER}}}{\left(\frac{\text{Sr}}{\text{Ca}}\right)_{\text{CM}}} = \frac{K_{\text{f}}}{1 + \frac{F_{\text{b}}}{F_{\text{ER}}+F_{\text{b}}}\left(\frac{K_{\text{f}}}{K_{\text{eq}}} - 1\right)} \tag{4b}$$

$$K_{\text{f-OUT}} = \frac{\left(\frac{\text{Sr}}{\text{Ca}}\right)_{\text{SW}}}{\left(\frac{\text{Sr}}{\text{Ca}}\right)_{\text{CM}}} = \frac{K_{\text{f}}}{1 + \frac{F_{\text{b}}}{F_{\text{OUT}}+F_{\text{b}}}\left(\frac{K_{\text{f}}}{K_{\text{eq}}} - 1\right)} \tag{4c}$$

Due to its larger ionic radius, Sr detachment from water molecules is easier compared to that of Ca (DePaolo, 2011). Therefore we assume that Sr transmembrane desolvation occurs faster than for Ca, implying that the forward kinetic partition coefficient for Sr/Ca (K_{f}) should be >1. There is a twofold difference in the dissolution rate between Sr and Ca carbonates, which could indicate a K_{f} difference of this order, but values as low as 1.1 have also been proposed from water exchange kinetics (Pokrovsky and Schott, 2002). For this model, we have used a forward kinetic partition coefficient (K_{f}) of 1.1 (Appendix A).

During transmembrane transport, the equilibrium Sr/Ca partition coefficient (K_{eq}) is assumed to be 1, given the lack of evidence of Sr or Ca preference by different Ca transporters (Allen and Sanders, 1994; Berman and King, 1990). As previously described for modeling $\Delta^{44/40}\text{Ca}_{\text{cocco-sw}}$, there is no theoretical constraint of F_{b} for Sr/Ca transport. Therefore, to keep the model simple, F_{b} was assumed to take the same value as used for $\Delta^{44/40}\text{Ca}_{\text{cocco-sw}}$ modeling (5×10^{-8} mol/m^2/s), which is in the range of values used by DePaolo (2011) for modeling results of other studies of Sr incorporation into abiogenic calcite. A sensitivity analysis of the model output when the F_{b} values of the transport steps from the cytosolic microenvironment to the endoplasmic reticulum and from the cytosolic microenvironment to seawater are varied, are shown in Appendix C.

Since Sr and Ca are thought to share the same cellular pathways (Müller et al., 2011), we model both ions in the same way. The only difference occurs after Sr and Ca are transported to the site of calcification (coccolith vesicle). At this stage, all the Ca is assumed to be fixed into calcite to cope with the high Ca demand for coccolith formation. On the other hand, only part of the transported Sr is fixed into calcite (effective Sr/Ca partition coefficient $K_{\text{lith}} < 1$). The Sr that is not fixed is assumed to be extruded into the cytosolic microenvironment as residual (F_{res}), producing an increase in its concentration there (Fig. 2a; Fig. 4b).

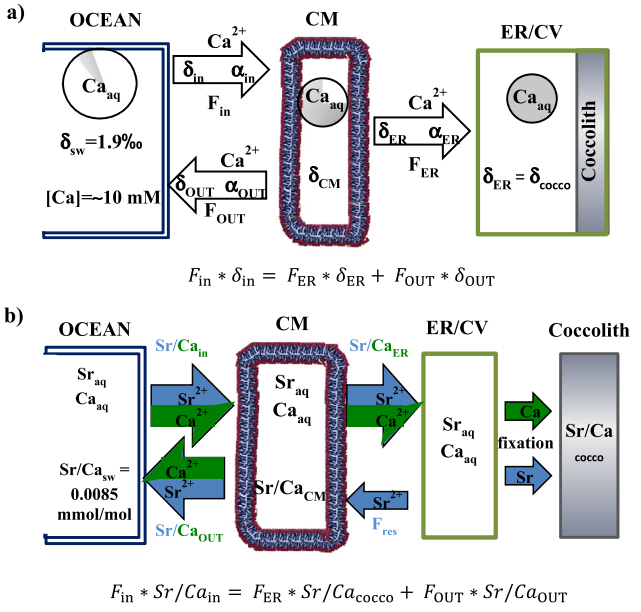

Fig. 4. CaSri–Co box model schematics illustrating Ca isotopic fractionation (a) and Sr/Ca (b) cellular dynamics in coccolithophores. Mass balance equations used for model construction are shown. In a) the effective Ca isotopic fractionation associated with 1) Ca transport from seawater to the cytosolic microenvironment – CM (α_{in}), 2) from the cytosolic microenvironment to the endoplasmic reticulum – ER (α_{ER}) and 3) from the cytosolic microenvironment to seawater (α_{OUT}), are illustrated. Seawater is an infinite reservoir (boundary condition) which $\delta^{44/40}$Ca and Sr/Ca (δ_{sw}, Sr/Ca$_{\text{sw}}$) are assumed to be constant, while $\delta^{44/40}$Ca and Sr/Ca of the cytosolic microenvironment reservoir (δ_{CM} and Sr/Ca$_{\text{CM}}$) are affected by the parameters of equations (3d) and (7e), respectively. The model shows that with every step in which a portion of the total Ca and Sr ions are desolvated (Ca_{aq}, Sr_{aq}: solvated; Ca^{2+}, Sr^{2+}: desolvated) and transported across membranes (F_{in}, F_{ER}, F_{OUT}), the $\delta^{44/40}$Ca (δ_{in}, δ_{ER}, δ_{OUT}) and Sr/Ca (Sr/Ca$_{\text{in}}$, Sr/Ca$_{\text{ER}}$, Sr/Ca$_{\text{OUT}}$) of the fluxes are successively modified. This affects the resulting $\delta^{44/40}$Ca and Sr/Ca measurements of the coccolith calcite (δ_{cocco} and Sr/Ca$_{\text{cocco}}$, respectively). In this model, the endoplasmic reticulum and the coccolith vesicle (CV) are considered as the same compartment (ER/CV), as we assume that all Ca and Sr in the endoplasmic reticulum are transferred to the coccolith vesicle. Once inside the coccolith vesicle, all Ca is assumed to be fixed (therefore $\delta_{\text{cocco}} = \delta_{\text{ER}}$), but part of the Sr is not and is transported back to the cytosolic microenvironment as a residual (Sr_{res}). In a) an approximation of the proportion of Ca_{aq} that is desolvated and transported/fixed is shown as partially-filled circles (for seawater and cytosolic microenvironment compartments) and as a filled circle (for the endoplasmic reticulum/coccolith vesicle/coccolith compartment). (For interpretation of the references to color in this figure legend, the reader is referred to the web version of this article.)

Inside the coccolith vesicle, partition coefficients during Sr incorporation into calcite depend to a large extent on calcification rates (F_{ER}). The effective Sr/Ca partition coefficient during calcite precipitation (K_{lith}) is described in Eq. (5). For the calcification step, we used an equilibrium Sr/Ca partition coefficient ($K_{\text{eq-lith}}$) of 0.07 and a forward kinetic partition coefficient for Sr/Ca ($K_{\text{f-lith}}$) of 0.24, as used by DePaolo (2011) to model the inorganic experimental data of Tang et al. (2008). The dissolution rate of coccolith calcite ($K_{\text{b}} = 2.5 \times 10^{-9}$ mol/m^2/s) was estimated assuming a coccolith vesicle solution Ca^{2+}:CO_3^{2-} stoichiometry of 1:0.2. This is in the range of the Ca and CO_3 concentrations reported by Holtz et al. (2015), following the K_{b} values reported in the model of Nielsen et al. (2012), and assuming that the growing coccolith surface area is 1/4 of the surface area through which Sr is taken up (Appendix A). The absolute value of Ca retention efficiency ($F_{\text{ER}}/F_{\text{in}}$) is sensitive to changes in the stoichiometry assumed for the calcifying fluid in the coccolith vesicle, and therefore to the K_{b} value. When K_{b} is increased by five times to a value of 1.25×10^{-8} mol/m^2/s, the average Ca retention efficiency required to model our Sr/Ca observational increases from 39 to 52% (Appendix D). Further ex-

perimental studies are required to better constrain the dissolution rate of coccolith calcite (K_b). The equation for the effective Sr/Ca partition coefficient during calcite precipitation is:

$$K_{lith} = \frac{K_{f\text{-}lith}}{1 + \frac{K_b}{F_{ER}+K_b}\left(\frac{K_{f\text{-}lith}}{K_{eq\text{-}lith}} - 1\right)} \quad (5)$$

This steady-state model assumes that the Ca (and Sr) ion fluxes into the cell (F_{in}) and its respective Sr/Ca ratios (Sr/Ca_{in}) are equal to the total Ca (and Sr) ion fluxes and their respective Sr/Ca ratios out of the cell (F_{ER} and Sr/Ca_{cocco}; F_{OUT} and Sr/Ca_{OUT}) (mass balance equation: Eq. (6); Fig. 4b). The Sr/Ca ratio across each transmembrane passage (Sr/Ca_{in}, Sr/Ca_{ER}, Sr/Ca_{OUT}) depends on the Sr/Ca of the reservoir from which ions are transported (seawater: Sr/Ca_{sw}; cytosolic microenvironment: Sr/Ca_{CM}) and the effective Sr/Ca partitioning associated with individual transport passages ($K_{f\text{-}in}$, $K_{f\text{-}ER}$, $K_{f\text{-}OUT}$) (Eqs. (7a), (7b), (7c)). Similarly, the Sr/Ca ratio of the finished coccolith (Sr/Ca_{cocco}) depends on the Sr/Ca of the reservoir from which ions are precipitated (endoplasmic reticulum/coccolith vesicle – ER/CV: Sr/Ca_{ER}) and the effective Sr/Ca partitioning associated with calcification (K_{lith}) (Eq. (7d)). K_{lith} determines the degree of Sr enrichment of the cytosolic microenvironment via transport of the non-fixed Sr from the coccolith vesicle.

We assume that the Sr/Ca of the seawater reservoir (Sr/Ca_{sw}) remains constant (0.0085 mol/mol; average value for an Atlantic Ocean transect; De Villiers, 1999), and is unaffected by ion uptake. On the other hand, the Sr/Ca of the cytosolic microenvironment (Sr/Ca_{CM}) shows an evolution as ions are transported/fixed into the coccolith calcite (Fig. 4b). Sr/Ca_{CM} is mathematically resolved by substituting the Sr/Ca_{OUT} and Sr/Ca_{cocco} terms of the mass balance equation (Eq. (6)) with the equations (7c) and (7d), and solving for Sr/Ca_{CM} (Eq. (7e)). The relevant mass balance equations are:

$$F_{in} * Sr/Ca_{in} = F_{ER} * Sr/Ca_{cocco} + F_{OUT} * Sr/Ca_{OUT} \quad (6)$$

$$Sr/Ca_{in} = Sr/Ca_{SW} * K_{f\text{-}in} \quad (7a)$$

$$Sr/Ca_{ER} = Sr/Ca_{CM} * K_{f\text{-}ER} \quad (7b)$$

$$Sr/Ca_{OUT} = Sr/Ca_{CM} * K_{f\text{-}OUT} \quad (7c)$$

$$Sr/Ca_{cocco} = Sr/Ca_{ER} * K_{lith} \quad (7d)$$

$$Sr/Ca_{CM} = \frac{F_{in} * Sr/Ca_{in}}{F_{OUT} * K_{f\text{-}OUT} + F_{ER} * K_{f\text{-}ER} * K_{lith}} \quad (7e)$$

4.2. Model constraints on coccolith $\Delta^{44/40}Ca_{cocco\text{-}sw}$ and Sr/Ca variation

The model suggests that calcification rate (F_{ER}) and Ca retention efficiency (F_{ER}/F_{in}) regulate Ca isotopic fractionation in coccolithophores ($\Delta^{44/40}Ca_{cocco\text{-}sw}$: coccolith $\delta^{44/40}Ca$ – seawater $\delta^{44/40}Ca$), although we cannot discard potential effects of other mechanisms not considered. Higher calcification rates reduce $\Delta^{44/40}Ca_{cocco\text{-}sw}$ in model simulations (Fig. 5a; Appendix C). For the simplest version of this model which assumes uniform F_b and α_{eq} across all transmembrane transport steps, Ca retention efficiency drives a ~0.3‰ range in $\Delta^{44/40}Ca_{cocco\text{-}sw}$ at a given calcification rate. Higher $\Delta^{44/40}Ca_{cocco\text{-}sw}$ values are observed at lower efficiencies, when these are in the range of values constrained by cultures (intermediate efficiencies) (Fig. 6). In Appendix E we describe the mechanisms for the dependence of $\Delta^{44/40}Ca_{cocco\text{-}sw}$ on a) calcification rate at constant Ca retention efficiency, and on b) Ca retention efficiency at constant calcification rates, in both cases for constant F_b and α_f.

For the simplest version of our model, the range of measured $\Delta^{44/40}Ca_{cocco\text{-}sw}$ of our *E. huxleyi* and *G. oceanica* cultures agrees best with the modeled range of $\Delta^{44/40}Ca_{cocco\text{-}sw}$ when an F_b of 5×10^{-8} mol/m^2/s and an α_f of 0.9982 (−1.802‰) is applied (Fig. 5a). The slope of the modeled dependence of $\Delta^{44/40}Ca_{cocco\text{-}sw}$ on calcification rate is low relative to the magnitude of the analytical error of $\delta^{44/40}Ca$ measurements. Nonetheless, for a given calcification rate, the range in $\Delta^{44/40}Ca_{cocco\text{-}sw}$ may reflect different Ca retention efficiencies among different culture experiments. $\Delta^{44/40}Ca_{cocco\text{-}sw}$ of *E. huxleyi* cultures from other studies where calcification rate is reported overall agree with the modeled trend of $\Delta^{44/40}Ca_{cocco\text{-}sw}$ and calcification rate (Fig. 5a). Results from *E. huxleyi* cultured at varying light intensities (Langer et al., 2007) fall largely within the modeled $\Delta^{44/40}Ca_{cocco\text{-}sw}$, except for the culture with the lowest calcification rate.

Our model also suggests an important role of the characteristics of the solvation environment (solution from which Ca is desolvated before being transported) driving changes in coccolith Ca isotopic fractionation. There are different factors that may influence the characteristics of the solvation environments in our model (i.e. seawater and the cytosolic microenvironment). These factors control the water structure strength (attraction strength between water molecules) and consequently, also influence the solvation (F_b) and desolvation (F_f) (hydration and dehydration) rates (Kowacz and Putnis, 2008), which in turn, drive changes in coccolith Ca isotopic fractionation. One of the factors controlling the water structure strength of the solvation environment (both seawater and cytosolic microenvironment) is temperature. Lower temperatures strengthen the water structure, decreasing F_b (Krestov and Kobenin, 1980). As temperature drops from 20 to 5 °C, an order of magnitude reduction in F_b in our model could explain the 0.45‰ decrease in $\Delta^{44/40}Ca_{cocco\text{-}sw}$ of the *E. huxleyi* cultures of Gussone et al. (2006) (Fig. 5b). The magnitude of this temperature effect on $\Delta^{44/40}Ca_{cocco\text{-}sw}$ is greater than the magnitude of the Ca retention efficiency effect on $\Delta^{44/40}Ca_{cocco\text{-}sw}$. Based on Fig. 5b, we suggest equations describing the temperature effect on F_b rates (Appendix F). Since our cultures and those of Langer et al. (2007) (Fig. 5a) were grown at similar temperatures (17–18 °C), the $\Delta^{44/40}Ca_{cocco\text{-}sw}$ variability observed cannot be explained by F_b changes linked to temperature variations.

Similarly, lower seawater Mg concentrations increase F_b through decreased water structure strength (Krestov and Kobenin, 1980). The lower Ca isotopic fractionation (higher $\Delta^{44/40}Ca_{cocco\text{-}sw}$) observed in the *E. huxleyi* cultured at Mg concentrations half those of normal seawater (Müller et al., 2011) (Fig. 5c) could in part reflect the expected higher F_b. In these cultures, variations of calcification rate or Ca retention efficiency alone cannot explain the observed differences in $\Delta^{44/40}Ca_{cocco\text{-}sw}$.

The presence of organic compounds also affects the properties of the solvation environment (Kowacz and Putnis, 2008). Though this aspect is not addressed in this study, the presence of organic molecules secreted by cells should be considered in future studies, as they may also affect F_b in cultures grown at constant temperature and seawater composition, potentially contributing to $\Delta^{44/40}Ca_{cocco\text{-}sw}$ variation. If significant, such factors would appear to have systematic relationships with factors such as calcification rate and CO_2, in order to contribute to the correlations observed between $\Delta^{44/40}Ca_{cocco\text{-}sw}$ and these parameters.

In model simulations, coccolith Sr/Ca increases significantly with increasing Ca retention efficiency (F_{ER}/F_{in}) (Fig. 6b) and to a lesser extent, with increasing calcification rates (Fig. 6a). The efficiency effect is due to the cytosolic microenvironment accumulation of the residual Sr that is not fixed in the coccolith vesicle, whereas the calcification rate effect is due to the rate dependence of the Sr partition coefficient (e.g. DePaolo, 2011). Given our assumptions of the dissolution rate of coccolith calcite ($K_b = 2.5 \times 10^{-9}$ mol/m^2/s), the absolute Sr/Ca ratios measured in cultures constrain Ca retention efficiencies to <50%. Among different

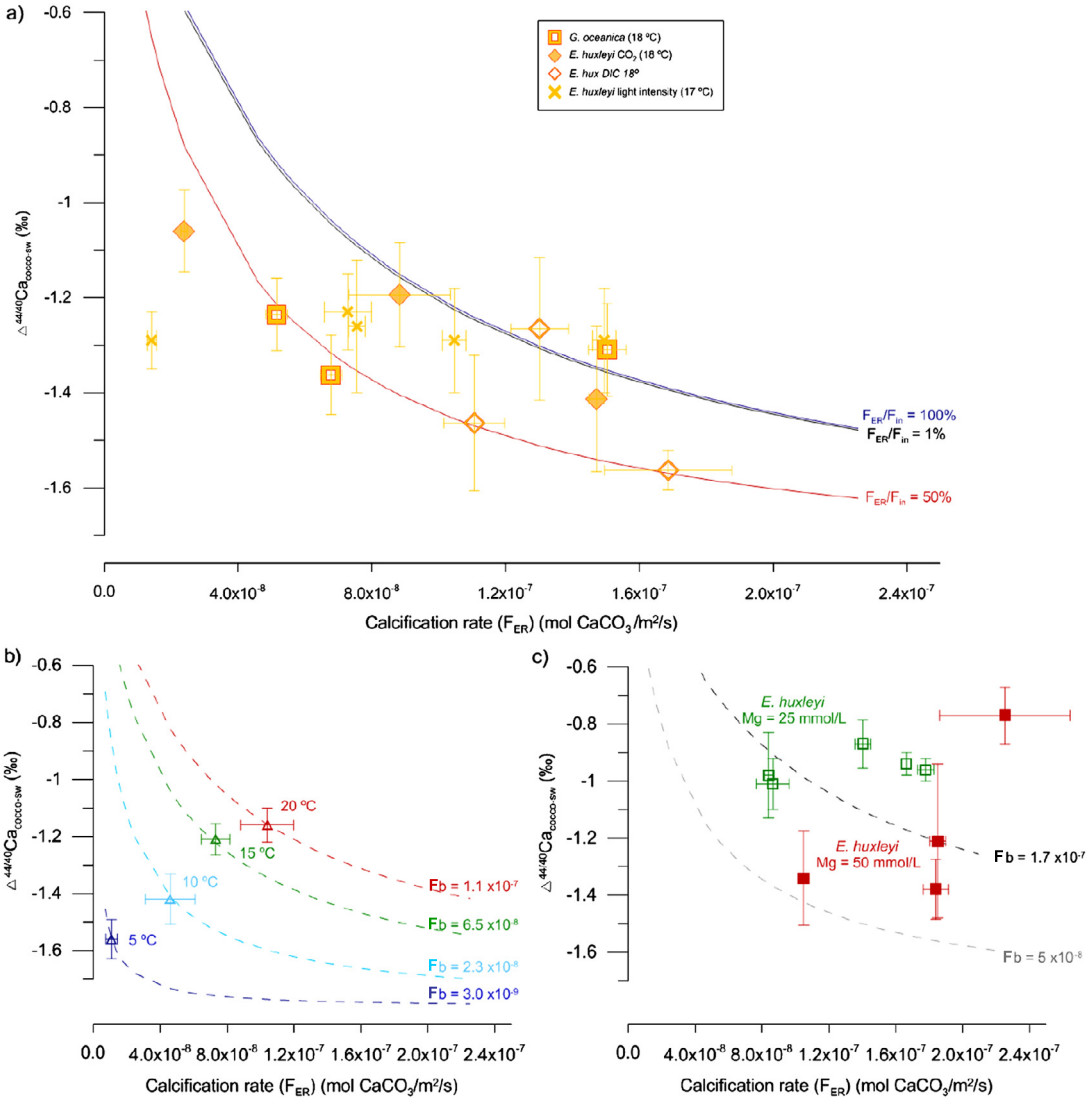

Fig. 5. Modeled Ca isotopic fractionation ($\Delta^{44/40}Ca_{cocco\text{-}sw}$ (‰)) as a function of calcification rate (F_{ER} (mol $CaCO_3/m^2/s$)) at a) varying Ca retention efficiencies (F_{ER}/F_{in} (%)), b) and c) constant F_{ER}/F_{in} of 40%. In a) a constant F_b of 5×10^{-8} mol/m^2/s was used to match the modeled and measured range of $\Delta^{44/40}Ca_{cocco\text{-}sw}$ of our *E. huxleyi* and *G. oceanica* cultures. Results of *E. huxleyi* from other studies cultured at similar temperatures and same Mg concentrations (Langer et al., 2007) are shown for comparison purposes. Minimum $\Delta^{44/40}Ca_{cocco\text{-}sw}$ are observed at $F_{ER}/F_{in} = 50\%$ (red), while increasing $\Delta^{44/40}Ca_{cocco\text{-}sw}$ are obtained either at $F_{ER}/F_{in} < 50\%$ (black) or $F_{ER}/F_{in} > 50\%$ (blue). In b) F_b values of 3.0×10^{-9}, 2.3×10^{-8}, 6.5×10^{-8} and 1.1×10^{-7} mol/m^2/s were used to obtain modeled $\Delta^{44/40}Ca_{cocco\text{-}sw}$ that match the average $\Delta^{44/40}Ca_{cocco\text{-}sw}$ measurements of *E. huxleyi* cultured at 5 (dark blue), 10 (light blue), 15 (green) and 20 °C (red) (Gussone et al., 2006), respectively. In c) a higher F_b value (1.7×10^{-7} mol/m^2/s; dashed black) was used to obtain a modeled $\Delta^{44/40}Ca_{cocco\text{-}sw}$ that matches the range of $\Delta^{44/40}Ca_{cocco\text{-}sw}$ measured in *E. huxleyi* cultured at low Mg concentrations (25 mmol/L; green) by Müller et al. (2011). $\Delta^{44/40}Ca_{cocco\text{-}sw}$ measurements from the same study at normal seawater Mg concentrations (50 mmol/L; red) are described better by the model when a lower F_b (5×10^{-8} mol/m^2/s; dashed light gray) is applied. $\Delta^{44/40}Ca_{cocco\text{-}sw}$ and calcification rate measurements include their respective standard deviations (1σ). The model uses a uniform maximum fractionation of desolvation (α_f) across all membranes of −1.802‰. The range of F_{ER} used for modeling comprises measurements of *E. huxleyi* and *G. oceanica* from this study and from others for which calcification rate has been reported. (For interpretation of the references to color in this figure legend, the reader is referred to the web version of this article.)

experiments, most culture data are consistent with Ca retention efficiencies varying from 31 to 45% (Fig. 6b). These values would be on average ∼13% higher if a higher K_b of calcite dissolution of 1.25×10^{-8} mol/m^2/s was assumed (Appendix D).

Ca retention efficiency changes have a much larger effect on Sr/Ca compared to $\Delta^{44/40}Ca_{cocco\text{-}sw}$. In our model construction, Ca retention efficiency (F_{ER}/F_{in}) depends on 1) the backwards flux (F_b) during Ca transport across Ca channels, which determines the magnitude of the Ca flux crossing the plasma membrane (F_{in}), and 2) coccolithophores' ability to transport out of the cell the excess of unused Ca contained in the cytosolic microenvironment. While F_b at the Ca channels depends on the chemistry at the docking site of transporters and in our model is given a constant value, regulation of ion cytosolic concentrations, such as Ca, fully depends on cellular physiology and biology. We found that when we run the model inversely to determine the Ca retention efficiency needed to obtain values of $\Delta^{44/40}Ca_{cocco\text{-}sw}$ and Sr/Ca similar to those measured in our cultures, the solution was mainly driven by Sr/Ca. In the inverse solution, the differences between the modeled and the measured $\Delta^{44/40}Ca_{cocco\text{-}sw}$ may reach up to ±0.18‰. Increasing the F_b and/or the α_{eq} associated with internal Ca transporters (i.e. pumps) leads to an improvement of the model fit to the measured $\Delta^{44/40}Ca_{cocco\text{-}sw}$ (Appendix C).

A comparison of the results of the simplest version of our model and culture data suggests that the steep inverse correlation between Sr/Ca and $\Delta^{44/40}Ca_{cocco\text{-}sw}$ observed in our *E. huxleyi* and *G. oceanica* cultures (Fig. 1f) may result predominantly from the effect of varying calcification rate. This is because Ca retention efficiency changes at constant calcification rates produce a lowered slope compared to observations (Fig. 6c). It is worthwhile to

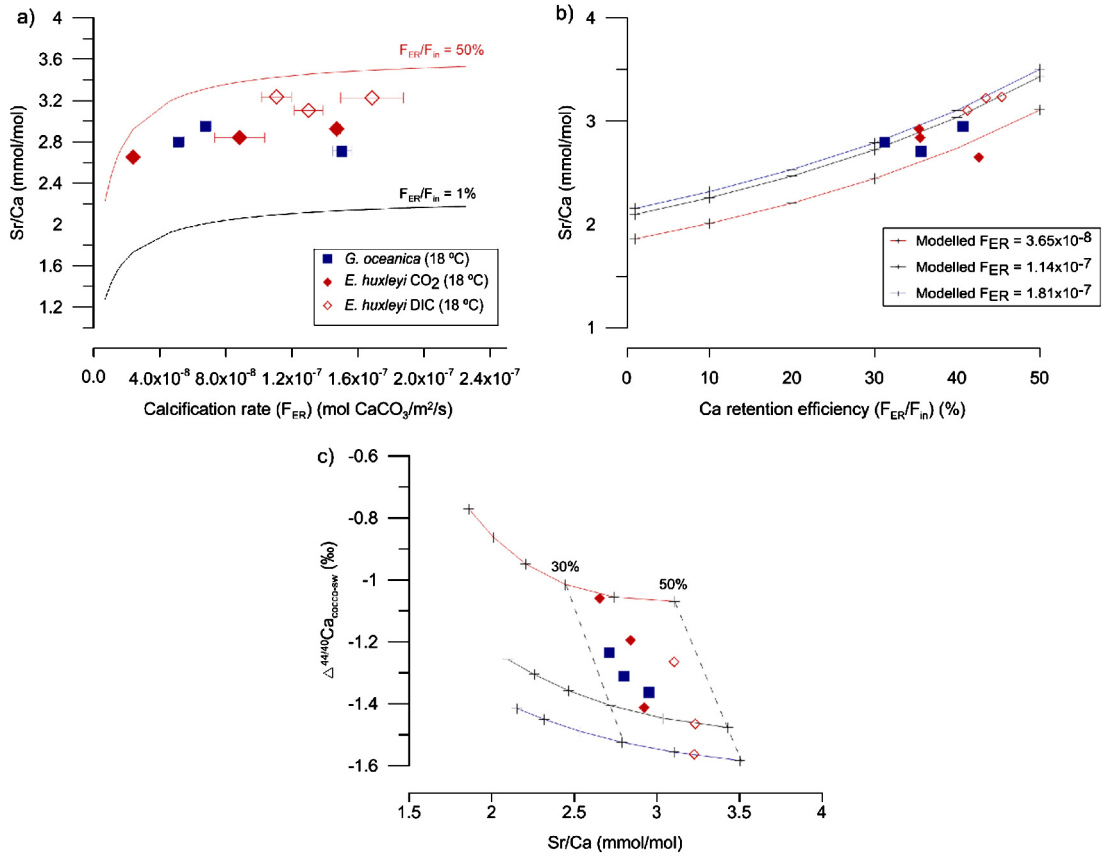

Fig. 6. a) Modeled Sr/Ca (mmol/mol) as a function of calcification rate (F_{ER} (mol $CaCO_3/m^2/s$)) at Ca retention efficiencies (F_{ER}/F_{in} (%)) varying from 1 (black) to 50% (red). b) Modeled Sr/Ca as a function of Ca retention efficiency at calcification rates varying from 3.65×10^{-8} (red) to 1.81×10^{-7} mol $CaCO_3/m^2/s$ (blue). The strong increasing effect of F_{ER}/F_{in} on coccolith Sr/Ca constrains retention efficiencies to values <50% when a dissolution rate of calcite (K_b) of 2.5×10^{-9} mol/m^2/s is used in the model. c) Modeled Ca isotopic fractionation ($\Delta^{44/40}Ca_{cocco\text{-}sw}$ (‰)) as a function of Sr/Ca at calcification rates varying from 3.65×10^{-8} (red) to 1.81×10^{-7} mol $CaCO_3/m^2/s$ (blue) as in b). The model produces an inverse relationship between $\Delta^{44/40}Ca_{ER}$ and Sr/Ca from low to moderate efficiencies, which agrees with observations from our cultured *E. huxleyi* and *G. oceanica* (Fig. 1f). Our culture results fall within Ca retention efficiencies varying from ~30 to ~50% (oblique black dashed lines). Measurements of Sr/Ca, calcification rates and $\Delta^{44/40}Ca_{cocco\text{-}sw}$, and modeled Ca retention efficiencies of *E. huxleyi* and *G. oceanica* from this study are shown for comparison purposes. (For interpretation of the references to color in this figure legend, the reader is referred to the web version of this article.)

note, however, that under three specific scenarios in which α_{eq} and/or F_b of internal transport steps were increased (Appendix C), steeper slopes for constant calcification rates were observed, agreeing better with the slope of observations. Thus it is not possible to uniquely attribute the mechanism of the negative correlation observed between Sr/Ca and $\Delta^{44/40}Ca_{cocco\text{-}sw}$. Due to the lack of reliable calcification rate measurements in our *C. leptoporus* cultures, it is not possible to identify the main driver of the observed insignificant positive logarithmic correlation between Sr/Ca and $\Delta^{44/40}Ca_{cocco\text{-}sw}$. However, the comparatively lower Sr/Ca of one of *C. leptoporus* cultures (2.15 mmol/mol), may imply that Ca retention efficiency in these culture may have been <31%.

5. Implications and considerations for paleo-studies

The CaSri–Co model elucidates important factors simultaneously regulating coccolith Ca isotopic fractionation and Sr/Ca, though there may be others not considered in this study. Increased calcification rates, Ca retention efficiencies (up to intermediate values) and water structure strength (lower F_b) raise both coccolith Sr/Ca and Ca isotopic fractionation. If significant temporal changes in coccolith Ca isotopic fractionation, such as those observed in our culture data (up to 0.5 ‰), occurred at times of high coccolith contribution to the global carbonate sink, it could impart temporal variation in seawater $\delta^{44/40}Ca$.

Though diagenesis of calcite has been suggested to slightly shift the original calcite $\delta^{44/40}Ca$ signal to heavier values, the maximum shift of $\delta^{44/40}Ca$ for sediments from Site 807A (Ontgong Java Plateau) was found to be 0.15‰ (Fantle and DePaolo, 2007). The magnitude of this shift remains small compared to the variability of $\delta^{44/40}Ca$ measured in our cultures (up to 0.5‰), and is in the range of analytical uncertainties. Moreover, the polysaccharides covering coccoliths make them less prone to dissolution/recrystallization processes compared to other biogenic carbonates (Chiu and Broecker, 2008), further limiting potential $\delta^{44/40}Ca$ shifts linked to diagenesis. Nonetheless, diagenetic recrystallization of sedimentary coccoliths can be assessed with scanning electron microscopy/light microscopy for $\delta^{44/40}Ca$ application to the sediment record. In spite of the potential for minor diagenetic effects on $\delta^{44/40}Ca$ (Fantle and DePaolo, 2007), a better understanding of the mechanisms controlling coccolith $\delta^{44/40}Ca$ and Sr/Ca through our model, will lead to a better interpretation of sedimentary $\delta^{44/40}Ca$ and its diagenetic history.

The observed high sensitivity of Sr/Ca to changes in Ca retention efficiency suggest a potential for elucidating how coccolithophores have varied their ability to retain Ca for calcification in the past from Sr/Ca measurements, if growth rate and seawater Sr/Ca were independently constrained. This information is crucial to disentangle coccolithophores' response and adaptation strategies to varying environmental conditions, which could have had implications on their contribution to global $CaCO_3$ production over time. Moreover, this finding increases our understanding of the basis controlling the coccolith Sr/Ca paleoproductivity proxy, de-

noting Ca retention efficiency as a further potential regulator of coccolith Sr/Ca variation.

Our model suggests that the characteristics of the solvation environment (i.e. water structure strength) may control $\Delta^{44/40}Ca_{cocco\text{-}sw}$ variation. The temperature effect reported by Gussone et al. (2007, 2006) could therefore be explained by changes in the energy with which water is attached to Ca in seawater, with lower temperatures increasing the energy of this bond and therefore decreasing F_b. This would imply that significant changes in sea surface temperature in past oceans could have caused substantial effects on coccolith $\Delta^{44/40}Ca_{cocco\text{-}sw}$. In addition to the direct effects of temperature on the water structure strength and coccolith Ca isotopic fractionation, temperature has been found to influence the composition of cellular membranes in coccolithophores (Brassell et al., 1986). Epithelial cell membranes with less hydrogen-bonding potential have been suggested to have a less favorable hydrophobic component to oppose desolvation energy for molecule transmembrane transport (Conradi et al., 1991). Therefore, we infer that coccolithophore membrane composition changes produced by varying past seawater temperature, may have also impacted coccolith $\Delta^{44/40}Ca_{cocco\text{-}sw}$ over time. This hypothesis remains to be assessed by future studies.

Increasing seawater Mg concentrations also strengthens the water structure and decreases F_b (Krestov and Kobenin, 1980). However, we infer that a doubling of Mg concentration is required to attain the 3.4-fold reduction in F_b observed in the *E. huxleyi* cultures from Müller et al. (2011) (Fig. 5c). Because the long residence time of Mg (~12 Ma) restricts Mg concentration variation on short timescales (only ~17.6% in the last ~12 Ma; Brennan et al., 2013), this factor could affect coccolith $\Delta^{44/40}Ca_{cocco\text{-}sw}$ only on much longer timescales. In contrast, temperature changes could produce more rapid effects on F_b.

Finally, here we introduce the hypothesis that coccolithophores may potentially modulate their own Ca isotopic fractionation via excretion of cellular organic compounds. These compounds could modify seawater properties in the near-cell microenvironment (or in the cytosolic microenvironment), potentially changing solvation–desolvation rates. Therefore, changes in the type or amount of cellular exudates (e.g. extracellular carbonic anhydrase or metal-binding proteins) produced in response to changing environmental conditions, and accompanying major shifts in cell physiology, could potentially have affected F_b and thus coccolith Ca isotopic fractionation.

6. Conclusions

The application of the CaSri–Co model to previously published and new $\delta^{44/40}$Ca and Sr/Ca results from cultured *E. huxleyi* and *G. oceanica*, has allowed us to conduct the first quantitative interpretation of coccolith Ca isotopic fractionation and achieve a better understanding of the potential mechanisms driving it. Given the importance of coccolith contribution to the global carbonate sink, large changes in their Ca isotopic fractionation in the past, such as those evidenced in our cultures (up to ~0.5‰), may have had implications in the past global Ca cycle.

The model shows increasing Sr/Ca and lower $\Delta^{44/40}Ca_{cocco\text{-}sw}$ at higher calcification rates, higher Ca retention efficiencies, and higher water structure strength (lower solvation–desolvation rates). While all Ca transported to the coccolith vesicle is used during calcification, the incomplete usage of Sr and subsequent Sr enrichment of the cytosolic microenvironment explains the especially large sensitivity of coccolith Sr/Ca to Ca retention efficiency changes. On the other hand, solvation–desolvation rates were found to have a larger effect on Ca isotopic fractionation.

The model allowed us to identify that apart from paleoproductivity, coccolith Sr/Ca could be a potential proxy of the efficiency with which coccolithophores are able to retain Ca for calcification in response to changing past environmental conditions. Specific drivers of Ca retention efficiency variability remain to be identified. We have also shown the role that changes in water structure strength may play in modulating coccolith past Ca isotopic fractionation. We suggest seawater temperature to be critical in modifying the desolvation energy required for Ca transmembrane transport, not only via changing F_b rates, but potentially also by modifying cell membrane composition. Finally, we propose that the variable production of cellular exudates excreted in response to changing environmental conditions could have contributed to variability in coccolith Ca isotopic fractionation. Though this hypothesis remains to be tested, it would help to explain the observed correlation between $\Delta^{44/40}Ca_{cocco\text{-}sw}$ and CO_2 in our cultures.

Author contributions

K.I. cultured the coccolithophores; L.A. cleaned the cultures; C.B. and A.M.-V. determined ε_{cocco} from cultured coccolithophores; L.M.M. and A.P. prepared samples for $\delta^{44/40}$Ca analysis; L.M.M. conducted the $\delta^{44/40}$Ca measurements under the supervision of A.K., F.B. and A.E.; H.M.S. and A.P. conceived the study of a relation between the Ca and the C systems in coccolithophores; H.M.S. and L.M.M. developed the Ca isotope and Sr/Ca cell model with contributions from F.B.; L.M.M. and H.M.S. wrote the paper with contribution from F.B., A.P., A.E. and C.B.

Acknowledgements

This investigation was funded by the National Science Foundation CAREER Grant OCE-0449732 to A.P., the European Community under the project ERC-STG-240222-PACE to H.M.S., and ETH Zurich (Leitzahl 09601). Manuel Prieto and Colin Brownlee are acknowledged for invaluable discussions on aqueous solvation and coccolithophore Ca acquisition, respectively.

Appendix A. Supplementary material

Supplementary material related to this article can be found online at https://doi.org/10.1016/j.epsl.2017.10.013.

References

Allen, G.J., Sanders, D., 1994. Two voltage-gated, calcium release channels coreside in the vacuolar membrane of broad bean guard cells. Plant Cell 6, 685–694. http://dx.doi.org/10.1105/tpc.6.5.685.

Bairbakhish, A.N., Bollmann, J., Sprengel, C., Thierstein, H.R., 1999. Disintegration of aggregates and coccospheres in sediment trap samples. Mar. Micropaleontol. 37, 219–223. http://dx.doi.org/10.1016/S0377-8398(99)00019-5.

Berman, M.C., King, S.B., 1990. Stoichiometries of calcium and strontium transport coupled to ATP and acetyl phosphate hydrolysis by skeletal sarcoplasmic reticulum. Biochim. Biophys. Acta 1029, 235–240. http://dx.doi.org/10.1016/0005-2736(90)90159-L.

Berry, L., Taylor, A.R., Lucken, U., Ryan, K.P., Brownlee, C., 2002. Calcification and inorganic carbon acquisition in coccolithophores. Funct. Plant Biol. 29, 289–299. http://dx.doi.org/10.1071/PP01218.

Bolton, C.T., Stoll, H.M., 2013. Late Miocene threshold response of marine algae to carbon dioxide limitation. Nature 500, 558–562. http://dx.doi.org/10.1038/nature12448.

Bourg, I.C., Richter, F.M., Christensen, J.N., Sposito, G., 2010. Isotopic mass dependence of metal cation diffusion coefficients in liquid water. Geochim. Cosmochim. Acta 74, 2249–2256. http://dx.doi.org/10.1016/j.gca.2010.01.024.

Brassell, S.C., Brereton, R.G., Eglinton, G., Grimalt, J., Liebezeit', G., Marlowe, I.T., Pflaumann, U., Sarnthein, M., 1986. Palaeoclimatic signals recognized by chemometric treatment of molecular stratigraphic data. Adv. Org. Geochem. 10, 649–660. http://dx.doi.org/10.1016/S0146-6380(86)80001-8.

Brennan, S.T., Lowenstein, T.K., Cendón, D.I., 2013. The major-ion composition of Cenozoic seawater: the past 36 million years from fluid inclusions in marine halite. Am. J. Sci. 313, 713–775. http://dx.doi.org/10.2475/08.2013.01.

Brownlee, C., Davies, M., Nimer, N., Dong, L.F., Merret, M.J., 1995. Calcification, photosynthesis and intracellular regulation in Emiliania huxleyi. Bull. Inst. Oceanogr. Monaco 14, 19–35.

Brownlee, C., Taylor, A., 2005. Calcification in coccolithophores: a cellular perspective. In: Thierstein, H.R., Young, J.R. (Eds.), Coccolithophores: From Molecular Processes to Global Impact. Springer, Berlin, pp. 31–50.

Burton, P.S., Conradi, R.A., Hilgers, A.R., Ho, N.F.H., Maggiora, L.L., 1992. The relationship between peptide structure and transport across epithelial cell monolayers. J. Control. Release 19, 87–98. http://dx.doi.org/10.1016/0168-3659(92)90067-2.

Camacho, C.J., Kimura, S.R., DeLisi, C., Vajda, S., 2000. Kinetics of desolvation-mediated protein–protein binding. Biophys. J. 78, 1094–1105. http://dx.doi.org/10.1016/S0006-3495(00)76668-9.

Chiu, T.-C., Broecker, W.S., 2008. Toward better paleocarbonate ion reconstructions: new insights regarding the $CaCO_3$ size index. Paleoceanography 23, PA2216. http://dx.doi.org/10.1029/2008PA001599.

Conradi, R.A., Hilgers, A.R., Ho, N.F.H., Burton, P.S., 1991. The influence of peptide structure on transport across Caco-2 cells. Pharm. Res. 8, 1453–1460. http://dx.doi.org/10.1016/S0006-3495(00)76668-9.

De La Rocha, C.L., DePaolo, D.J., 2000. Isotopic evidence for variations in the marine calcium cycle over the Cenozoic. Science 289, 1176–1178. http://dx.doi.org/10.1126/science.289.5482.1176.

De Villiers, S., 1999. Seawater strontium and Sr/Ca variability in the Atlantic and Pacific oceans. Earth Planet. Sci. Lett. 171, 623–634. http://dx.doi.org/10.1016/S0012-821X(99)00174-0.

DePaolo, D.J., 2011. Surface kinetic model for isotopic and trace element fractionation during precipitation of calcite from aqueous solutions. Geochim. Cosmochim. Acta 75, 1039–1056. http://dx.doi.org/10.1016/j.gca.2010.11.020.

Dickson, A.G., Millero, F.J., 1987. A comparison of the equilibrium constants for the dissociation of carbonic acid in seawater media. Deep-Sea Res. A 34, 1733–1743. http://dx.doi.org/10.1016/0198-0149(87)90021-5.

Fantle, M.S., 2010. Evaluating the Ca isotope proxy. Am. J. Sci. 310, 194–230. http://dx.doi.org/10.2475/03.2010.03.

Fantle, M.S., DePaolo, D.J., 2007. Ca isotopes in carbonate sediment and pore fluid from ODP Site 807A: the Ca^{2+}_{aq}-calcite equilibrium fractionation factor and calcite recrystallization rates in Pleistocene sediments. Geochim. Cosmochim. Acta 71, 2524–2546. http://dx.doi.org/10.1016/j.gca.2007.03.006.

Fantle, M.S., Tipper, E.T., 2014. Calcium isotopes in the global biogeochemical Ca cycle: implications for development of a Ca isotope proxy. Earth-Sci. Rev. 129, 148–177. http://dx.doi.org/10.1016/j.earscirev.2013.10.004.

Fantle, M.S., Tollerud, H., Eisenhauer, A., Holmden, C., 2012. The Ca isotopic composition of dust-producing regions: measurements of surface sediments in the Black Rock Desert, Nevada. Geochim. Cosmochim. Acta 87, 178–193. http://dx.doi.org/10.1016/j.gca.2012.03.037.

Griffith, E.M., Paytan, A., Caldeira, K., Bullen, T.D., Thomas, E., 2008. A dynamic marine calcium cycle during the past 28 million years. Science 322, 1671–1674. http://dx.doi.org/10.1126/science.1163614.

Gussone, N., Eisenhauer, A., Heuser, A., Dietzel, M., Bock, B., Böhm, F., Spero, H.J., Lea, D.W., Bijma, J., Nägler, T.F., 2003. Model for kinetic effects on calcium isotope fractionation (δ^{44}Ca) in inorganic aragonite and cultured planktonic foraminifera. Geochim. Cosmochim. Acta 67, 1375–1382. http://dx.doi.org/10.1016/S0016-7037(02)01296-6.

Gussone, N., Langer, G., Geisen, M., Steel, B.A., Riebesell, U., 2007. Calcium isotope fractionation in coccoliths of cultured Calcidiscus leptoporus, Helicosphaera carteri, Syracosphaera pulchra and Umbilicosphaera foliosa. Earth Planet. Sci. Lett. 260, 505–515. http://dx.doi.org/10.1016/j.epsl.2007.06.001.

Gussone, N., Langer, G., Thoms, S., Nehrke, G., Eisenhauer, A., Riebesell, U., Wefer, G., 2006. Cellular calcium pathways and isotope fractionation in Emiliania huxleyi. Geology 34, 625–628. http://dx.doi.org/10.1130/G22733.1.

Heuser, A., Eisenhauer, A., Gussone, N., Bock, B., Hansen, B.T., Nägler, T.F., 2002. Measurement of calcium isotopes (δ^{44}Ca) using a multicollector TIMS technique. Int. J. Mass Spectrom. 220, 385–397. http://dx.doi.org/10.1016/S1387-3806(02)00838-2.

Hofmann, A.E., Bourg, I.C., DePaolo, D.J., 2012. Ion desolvation as a mechanism for kinetic isotope fractionation in aqueous systems. Proc. Natl. Acad. Sci. USA 109, 18689–18694. http://dx.doi.org/10.1073/pnas.1208184109.

Holtz, L.M., Thoms, S., Langer, G., Wolf-Gladrow, D.A., 2013. Substrate supply for calcite precipitation in Emiliania huxleyi: assessment of different model approaches. J. Phycol. 49, 417–426. http://dx.doi.org/10.1111/jpy.12052.

Holtz, L.-M., Wolf-Gladrow, D., Thoms, S., 2015. Numerical cell model investigating cellular carbon fluxes in Emiliania huxleyi. J. Theor. Biol. 364, 305–315. http://dx.doi.org/10.1016/j.jtbi.2014.08.040.

Keller, M.D., Selvin, R.C., Claus, W., Guillard, R.R.L., 1987. Media for the culture of oceanic ultraphytoplankton. J. Phycol. 23, 633–638. http://dx.doi.org/10.1111/j.1529-8817.1987.tb04217.x.

Kısakürek, B., Eisenhauer, A., Böhm, F., Hathorne, E.C., Erez, J., 2011. Controls on calcium isotope fractionation in cultured planktic foraminifera, Globigerinoides ruber and Globigerinella siphonifera. Geochim. Cosmochim. Acta 75, 427–443. http://dx.doi.org/10.1016/j.gca.2010.10.015.

Klibanov, A.M., 2001. Improving enzymes by using them in organic solvents. Nature 409, 241–246. http://dx.doi.org/10.1038/35051719.

Kowacz, M., Putnis, A., 2008. The effect of specific background electrolytes on water structure and solute hydration: consequences for crystal dissolution and growth. Geochim. Cosmochim. Acta 72, 4476–4487. http://dx.doi.org/10.1016/j.gca.2008.07.005.

Krestov, G.A., Kobenin, V.A., 1980. From Crystal to Solution. Mir Publishers Central Books Ltd, Moscow.

Langer, G., Gussone, N., Nehrke, G., Riebesell, U., Eisenhauer, A., Thoms, S., 2007. Calcium isotope fractionation during coccolith formation in Emiliania huxleyi: independence of growth and calcification rate. Geochem. Geophys. Geosyst. 8, Q05007. http://dx.doi.org/10.1029/2006GC001422.

Lemarchand, D., Wasserburg, G.J., Papanastassiou, D.A., 2004. Rate-controlled calcium isotope fractionation in synthetic calcite. Geochim. Cosmochim. Acta 68, 4665–4678. http://dx.doi.org/10.1016/j.gca.2004.05.029.

Lewis, E., Wallace, D., 1998. Program Developed for CO_2 System Calculations, ORNL/CDIAC-105. Carbon Dioxide Information Analysis Center, Oak Ridge National Laboratory, US Department of Energy, Oak Ridge, TN.

Mackinder, L., Wheeler, G., Schroeder, D., Riebesell, U., Brownlee, C., 2010. Molecular mechanisms underlying calcification in coccolithophores. Geomicrobiol. J. 27, 585–595. http://dx.doi.org/10.1080/01490451003703014.

Mackinder, L., Wheeler, G., Schroeder, D., von Dassow, P., Riebesell, U., Brownlee, C., 2011. Expression of biomineralization-related ion transport genes in Emiliania huxleyi. Environ. Microbiol. 13, 3250–3265. http://dx.doi.org/10.1111/j.1462-2920.2011.02561.x.

Mehrbach, C., Culberson, C.H., Hawley, J.E., Pytkowicx, R.M., 1973. Measurement of the apparent dissociation constants of carbonic acid in seawater at atmospheric pressure. Limnol. Oceanogr. 18, 897–907. http://dx.doi.org/10.4319/lo.1973.18.6.0897.

Mejía, L.M., Ziveri, P., Cagnetti, M., Bolton, C., Zahn, R., Marino, G., Martínez-Méndez, G., Stoll, H.M., 2014. Effects of midlatitude westerlies on the paleoproductivity at the Agulhas Bank slope during the penultimate glacial cycle: evidence from coccolith Sr/Ca ratios. Paleoceanography 29, 697–714. http://dx.doi.org/10.1002/2013PA002589.

Milliman, J.D., 1993. Production and accumulation of calcium carbonate in the ocean: budget of a nonsteady state. Glob. Biogeochem. Cycles 7, 927–957. http://dx.doi.org/10.1029/93GB02524.

Müller, M.N., Barcelos e Ramos, J., Schulz, K.G., Riebesell, U., Kaźmierczak, J., Gallo, F., Mackinder, L., Li, Y., Nesterenko, P.N., Trull, T.W., Hallegraeff, G.M., 2015. Phytoplankton calcification as an effective mechanism to alleviate cellular calcium poisoning. Biogeosciences 12, 6493–6501. http://dx.doi.org/10.5194/bg-12-6493-2015.

Müller, M.N., Kısakürek, B., Buhl, D., Gutperlet, R., Kolevica, A., Riebesell, U., Stoll, H.M., Eisenhauer, A., 2011. Response of the coccolithophores Emiliania huxleyi and Coccolithus braarudii to changing seawater Mg^{2+} and Ca^{2+} concentrations: Mg/Ca, Sr/Ca ratios and $\delta^{44/40}$Ca, $\delta^{26/24}$Mg of coccolith calcite. Geochim. Cosmochim. Acta 75, 2088–2102. http://dx.doi.org/10.1016/j.gca.2011.01.035.

Nielsen, L.C., DePaolo, D.J., De Yoreo, J.J., 2012. Self-consistent ion-by-ion growth model for kinetic isotopic fractionation during calcite precipitation. Geochim. Cosmochim. Acta 86, 166–181. http://dx.doi.org/10.1016/j.gca.2012.02.009.

Pokrovsky, O.S., Schott, J., 2002. Surface chemistry and dissolution kinetics of divalent metal carbonates. Environ. Sci. Technol. 36, 426–432. http://dx.doi.org/10.1021/es010925u.

Popp, B.N., Laws, E.A., Bidigare, R.R., Dore, J.E., Hanson, K.L., Wakeham, S.G., 1998. Effect of phytoplankton cell geometry on carbon isotopic fractionation. Geochim. Cosmochim. Acta 62, 69–77. http://dx.doi.org/10.1016/S0016-7037(97)00333-5.

Spötl, C., 2005. A robust and fast method of sampling and analysis of δ^{13}C of dissolved inorganic carbon in ground waters. Isot. Environ. Health Stud. 41, 217–221. http://dx.doi.org/10.1080/10256010500230023.

Stoll, H.M., Langer, G., Shimizu, N., Kanamaru, K., 2012. B/Ca in coccoliths and relationship to calcification vesicle pH and dissolved inorganic carbon concentrations. Geochim. Cosmochim. Acta 80, 143–157. http://dx.doi.org/10.1016/j.gca.2011.12.003.

Tang, J., Dietzel, M., Böhm, F., Köhler, S.J., Eisenhauer, A., 2008. Sr^{2+}/Ca^{2+} and $^{44}Ca/^{40}Ca$ fractionation during inorganic calcite formation: II. Ca isotopes. Geochim. Cosmochim. Acta 72, 3733–3745. http://dx.doi.org/10.1016/j.gca.2008.05.033.

Trimborn, S., Wolf-Gladrow, D., Richter, K.U., Rost, B., 2009. The effect of pCO_2 on carbon acquisition and intracellular assimilation in four marine diatoms. J. Exp. Mar. Biol. Ecol. 376, 26–36. http://dx.doi.org/10.1016/j.jembe.2009.05.017.

Wescott, C.R., Noritomi, H., Klibanov, A.M., 1996. Rational control of enzymatic enantioselectivity through solvation thermodynamics. J. Am. Chem. Soc. 118, 10365–10370. http://dx.doi.org/10.1021/ja961394q.

Zeebe, R.E., Wolf-Gladrow, D., 2001. CO_2 in Seawater: Equilibrium, Kinetics, Isotopes. Elsevier Oceanography Series. Elsevier, Amsterdam.